SECTION 16. THE INTERACTION OF RADIATION WITH MATERIALS

16.1 INTRODUCTION

Previous sections have described the radiation environment to which Earth-orbiting electronic devices may be exposed, and have indicated how these devices react to that exposure. It will now be useful to describe the physical principles which govern the transfer of energy from the incoming radiation flux to the device materials. Of fundamental importance in this respect is the estimation of the attenuating effect of other materials protecting the device from the external radiation environment. This protection may be provided fortuitously ("built-in absorber") by spacecraft structural members or covers, or may have to be added specifically for protection ("add-on absorber").

This section describes some of the physical processes involved in radiation transport through matter, its attenuation, scattering and generation of secondary radiation.

Radiation attenuation data for the most important parts of the Earth's radiation environment are given in graphical form. These data should allow evaluation of radiation doses in simple geometries, given the input electron and proton energy spectra.

These data supersede those presented by Holmes-Siedle and Freeman (1978).

Subsequent sections will discuss ways of making the best use of shielding material at minimum cost and weight penalty, and describe computerised methods which deal with the complexity of some radiation-dose calculations for spacecraft.

16.2 PARTICLE RADIATION TRANSPORT

Energetic particles passing through material can undergo a variety of interactions leading to energy-loss, scattering and/or the generation of secondary particles. In Section 3 it was seen that the principal components of the Earth's radiation environment are energetic electrons and protons. Interactions involving these particles are summarised below.

16.3 ELECTRONS

Electrons interact with material mainly at the atomic level, producing excitation and ionisation while losing energy and being scattered in the process. Because of their low mass relative to nuclei, electrons are readily scattered through large angles and complete "backscattering" of electrons from materials can be significant, especially in high-Z materials. Electron acceleration in the strong electric fields of the atom result in the generation of energetic photons, a process known as "bremsstrahlung" (braking radiation).

Figure 16.1 illustrates electron/bremsstrahlung behaviour in matter. Electron and bremsstrahlung photon trajectories are shown in both aluminium and in lead. These trajectories were computed by Daly using the CERN Monte-Carlo code GEANT (see Section 18 for a discussion of computational methods). The figure shows clearly the tortuous nature of electron motion and the production of penetrating bremsstrahlung. Lead is clearly a better absorber of electrons than aluminium.

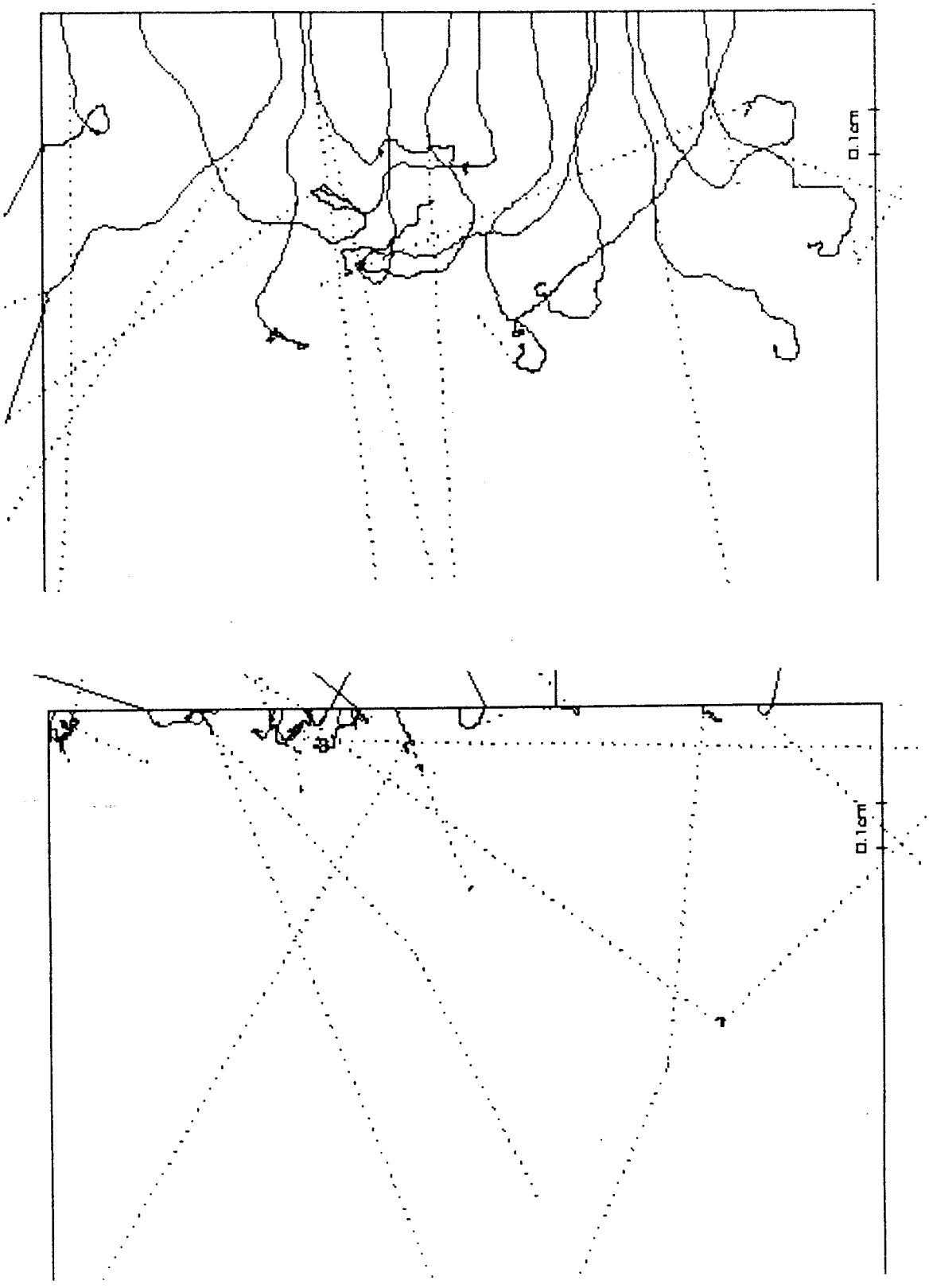

Trajectories of 5 MeV electrons in (a) aluminium and (b) lead as computed with the GEANT Monte-Carlo code. Electrons are injected normally from above. Dotted lines indicate the paths of bremsstrahlung photons induced by the electrons.

FIGURE 16.1

16.3.1 Transmission coefficients for electrons

We have already indicated that the transmission of electrons through material is a highly complex process. They do not travel in continuous straight lines, but follow highly scattered paths. The degree of scattering depends, for example, upon the material, the incident particle energy and the angle of incidence. A number of sophisticated analytical treatments have been developed to estimate the dose deposited and the residual flux after transmission of electrons through material of given "stopping power". Among the best known are the various "Monte Carlo" methods, whereby an electron track through a material is divided into a large number of "steps" very similar to the real case. In a typical treatment of an aluminium medium, as described by Berger & Seltzer (1968), the step size is chosen such that the electron energy decreases on average by a factor of 2^{-8} per step.

When a stream of "mono-energetic" electrons passes through a material, the energy and particle flux are both reduced. The emergent energy spectrum is broadened and somewhat asymmetric; however, a clearly dominant peak or "most probable energy" is preserved and its value will be less than the incident energy.

Number Transmission Coefficient (NTC) is the ratio between the total emergent particle fluence N_e and the total incident particle fluence, N_i :

$$NTC = N_e/N_i \qquad \text{.....16(i)}$$

Values of NTC for the transmission of omnidirectional electrons of energy 0 - 6 MeV through plane aluminium shielding of various thicknesses are tabulated by Berger & Seltzer (1968). These values are derived from the work of Hardy et al (1967) at NASA.

Figure 16.2 shows a graphical presentation of values of NTC as a function of aluminium absorber thickness (actually mass thickness in g. cm^{-2}) for various incident energies. A feature of each curve is the "tail", an effect of "straggling electrons" which penetrate further than might otherwise be expected. The tails of the curves cut the thickness axis at the "maximum range" for a particular energy. The broken lines, which neglect the straggling effect, cut the axis at the "Practical range". The practical ranges indicated in Figure 16.2 agree well with those given for aluminium by, for example, Linnenbom (1962).

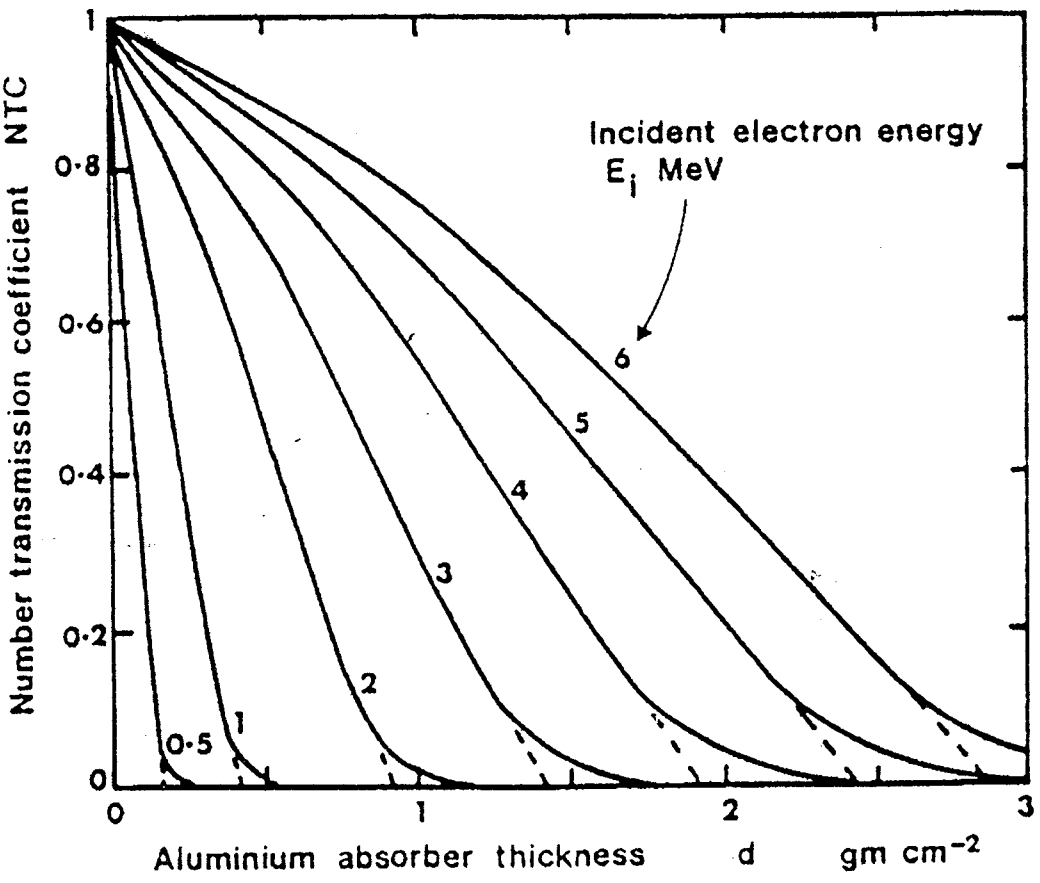

Number Transmission Coefficient (NTC) of omnidirectional electrons through plane aluminium absorber as a function of thickness.

FIGURE 16.2 - ELECTRON TRANSMISSION

16.3.2 Stopping power

For electrons in the energy range less than 5 MeV, typical of the Earth's trapped radiation belts, almost all energy loss during passage through material is by interaction mechanisms that result in ionisation of the material, i.e. the creation of electron-hole pairs with no momentum transfer to the atoms. The rate of loss of energy with distance traversed, known as the "stopping power" of the material, is given by the following equation (Berger and Seltzer, 1982):

$$\frac{dE}{dx} = \frac{2\pi e^4 z^2 N_A Z}{mv^2 A} .Be \qquad .....16(ii)$$

when ρN_A is the number of atoms per unit volume, where N_A ($\sim 6 \times 10^{23}$) is Avogadro's number atoms/mole, v is the velocity of the electron, e and m are the charge and mass of an electron, and x = "path length" or distance measured along the track of an electron.

B_e is known as the "electron stopping number" of the material; it is a function of particle energy, but rises only slowly with E. Therefore, dE/dx at first falls rapidly with increasing E (and hence v), being dominated by the $1/v^2$ dependence. It reaches a minimum as v approaches a limit at the speed of light. At higher energies (corresponding to a relativistic increase in electron mass), dE/dx rises slowly with the now dominant B dependence, since v is now limited.

The minimum stopping power for electrons occurs at energies in the range 1 - 2 MeV; electrons at this energy are said to be "minimum ionising". The amount of data available on stopping power for various materials is considerable (Berger & Seltzer, 1982). Note that, normally, stopping power is quoted in units of energy lost per unit "mass thickness" measured along the particle path in $MeV.g^{-1}.cm^2$ $\left(\frac{1}{\rho}\frac{dE}{dx}\right)$.

In addition to energy loss by collision, there is a further contribution to stopping power due to radiation loss (i.e. bremsstrahlung generation). At energies below 1 MeV, this is extremely small when compared with collision loss as a mechanism for stopping electrons. It is a rising function of energy, but does not dominate over collision loss except at energies well over 10 MeV. For the typical near-Earth electron spectrum (1 - 4 MeV), only a very small fraction of the energy passes into bremsstrahlung, but the latter radiation is so much more penetrating that it emerges as a significant remaining "background" when all electrons have been stopped.

16.3.3 Internal spectrum

The energy spectrum of the particle radiation emerging from the inner surface of an absorber will clearly be a degraded form of the incident external spectrum. Particles of lower energy, having ranges less than the shield thickness, may be completely stopped while at higher energies there will be a reduction in flux.

Figure 16.3 shows the effect on a flat incident isotropic electron spectrum of planar aluminium shielding. This behaviour was computed with the ITS/Tiger Monte-Carlo code by Daly. The change in the electron spectrum is shown in Figure 16.3(a), while Figure 16.3(b) shows how the emerging spectrum depends on direction.

Note that the fluxes shown are normalised to unit incident current and are differential in energy. On average, it takes 4 electrons distributed isotropically to produce unit current, 2 of which are moving away from the medium. In addition to this, 20 groups are used, each with a width of 0.25 MeV. Therefore, the unshielded flux is 0.4 electrons/MeV/unit incident current (20 X 0.4 X 0.25 MeV = 2 electrons).

Figure 16.3(a) shows that with small amounts of shielding, the upper edge of the spectrum is degraded but that this is accompanied by an enhancement of the low-energy portion of the spectrum, because of secondary electrons. As the shielding increases, both low and high-energy electrons are attenuated and lose energy, producing a rounding of the spectrum. Figure 16.3(b) shows that a significant fraction of the emerging electron flux is at relatively large angles to the normal direction.

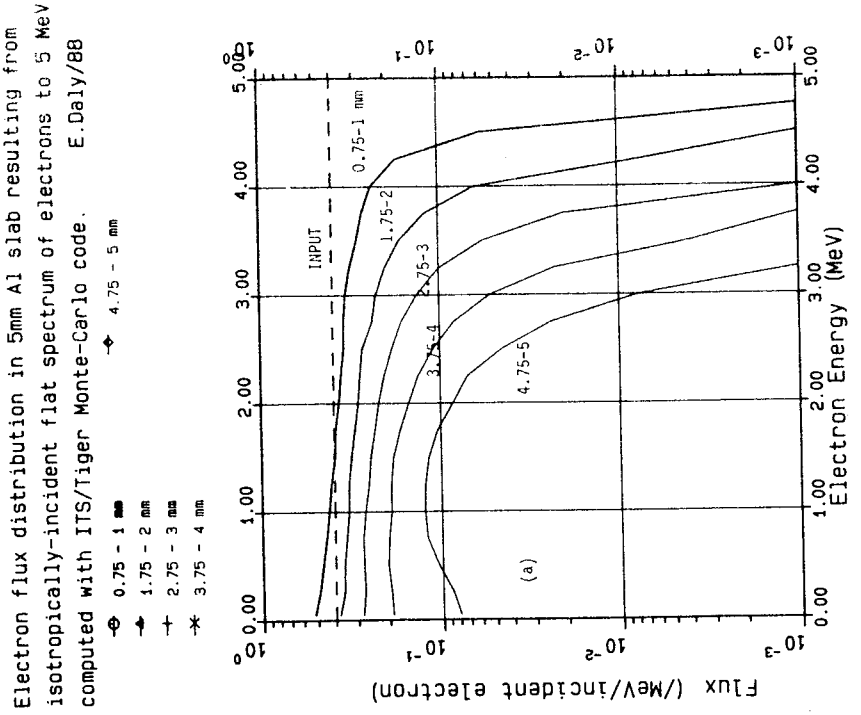

A

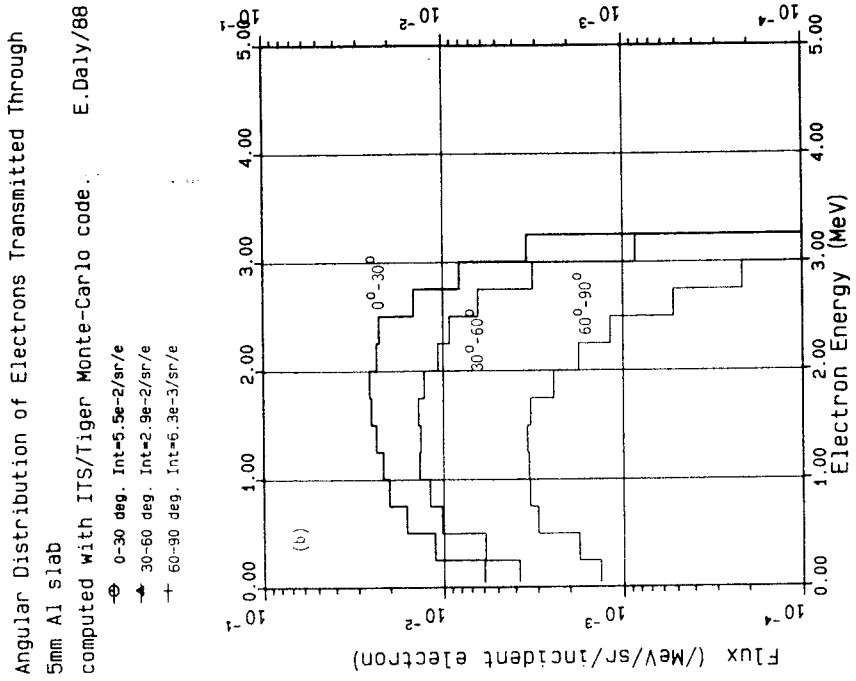

B

Variation of electron spectra in a 5mm slab. The input electrons are isotropic, with a uniform spectrum up to 5 MeV (indicated by the dotted line in (a)). (a) shows spectra at various depths. The fluxes are differential in energy and normalised to unit incident current. (b) shows the transmitted spectra in three ranges of angles to the slab normal. These fluxes are differential in both energy and solid angle.

FIGURE 16.3

16.4 ELECTROMAGNETIC RADIATION - BREMSSTRAHLUNG, X AND GAMMA RAYS

In spacecraft engineering and operations, energetic electromagnetic radiation can be encountered in a number of forms:

(a) Bremsstrahlung radiation produced by the slowing of energetic electrons in the atomic electric fields of a material. The electrons may be either from the space environment or from ground-testing electron beams.

(b) X-radiation produced by electron-beam excitation of atomic transitions.

(c) Nuclear emissions, Cerenkov radiation, etc..

The interaction of electromagnetic radiation with matter is thus a topic of some importance to those predicting or testing the response of devices to radiation, particularly where device electrode materials of high atomic number, such as gold and molybdenum, lie in close relation to the active region of the device. A discussion of the relevant general features of interactions is given here, while discussions of specific problems such as dose enhancement and package attenuation are given in other sections.

Since bremsstrahlung, X-rays and other electromagnetic radiation are just differing manifestations of the same type of radiation, they are absorbed according to the same laws. However, whereas bremsstrahlung is usually spread over a broad spectrum, X-rays and gamma-rays have well-defined energies, corresponding to atomic and nuclear energy states.

16.4.1 Bremsstrahlung

Photons produced by the bremsstrahlung mechanism are a significant problem in space applications because the ranges of the photons are generally greater than those of the primary electrons themselves. The production of bremsstrahlung is higher in materials of high atomic number, Z, and is proportional to the square of Z. Bremsstrahlung attenuation depends strongly on energy; photoelectric absoption usually dominates at energies below 0.1 MeV, Compton scattering at energies around 1 MeV and pair-production at high energy, above 10 MeV. These processes all result in the production of further electrons.

Figure 16.4(a) shows the bremsstrahlung spectra resulting from the flat electron spectrum shown in Figure 16.3(a). These were also produced with the ITS/TIGER Monte-Carlo code by Daly. Clearly there is a bias towards the production of low-energy photons, and while the shielding is less than the electron range, the continuing

production of bremsstrahlung leads to an increasing photon flux. Figure 16.4(a) shows that a significant fraction of the transmitted bremsstrahlung photon flux is at large angles from the slab normal.

16.4.2 X-rays

X-rays are produced by electron transitions in the atom. These can be stimulated by bombardment of material by an energetic electron beam, as occurs in X-ray tubes.

16.4.3 Other electromagnetic radiation

In passing through optical materials, energetic charged particles can also give rise to Cerenkov radiation. This is a result of particles travelling faster than the speed of light in the medium; the result is electromagnetic radiation emission which may interfere with the optical system's detectors.

Nuclear interactions can also give rise to gamma-radiation which can be troublesome, as mentioned in the next subsection.

Finally, gamma-radiation will be present if radioisotopes are used on-board a spacecraft. For example, radioisotope thermoelectric generators are used in deep-space interplanetary missions.

16.4.4 Production and attenuation of electromagnetic radiation

16.4.4.1 Production

Figure 16.5 (from Wayard) shows the spectrum of bremsstrahlung X-ray photons generated when a 1 MeV electron beam strikes a considerable thickness of material. As described later, this broad spectrum results from a complex process, but it will be seen that the peak of the spectrum emitted is at a photon energy of about half the energy of the impinging particle. Because it is broad, the emission is sometimes called "White Radiation".

Bremsstrahlung-generating efficiency is strongly dependent upon material; a heavy element will generate bremsstrahlung much more effectively than a lighter one. This efficiency is roughly in proportion to the atomic number. This dependence is not followed so simply, however, when attenuation of bremsstrahlung is dealt with, as described below.

Superimposed on the white radiation described above are the characteristic emission lines of the target material concerned. Table 16(1) gives some wavelengths for common target materials. For most materials, the cluster of K lines will be of greatest interest to us. However, for tantalum, tungsten, gold, platinum and lead, the L lines, which have photon energies in the 7-10 keV region, may also be of significance, especially in testing practices.

Figure 16.6 shows the photon spectra for a tungsten target on a commercial radiographic X-ray machine. The K emission appears as a complex set of lines. It can be seen that a copper filter greatly modifies or "hardens" the spectrum and reduces the influence of the characteristic lines.

Figure 16.7 shows another spectrum for a low-energy X-ray tube operating at 25kV. Here, the 'L' lines are seen and, because of the low beam voltage, the K lines are not excited. Both types of X-ray tube are currently being used for device testing (see later sections).

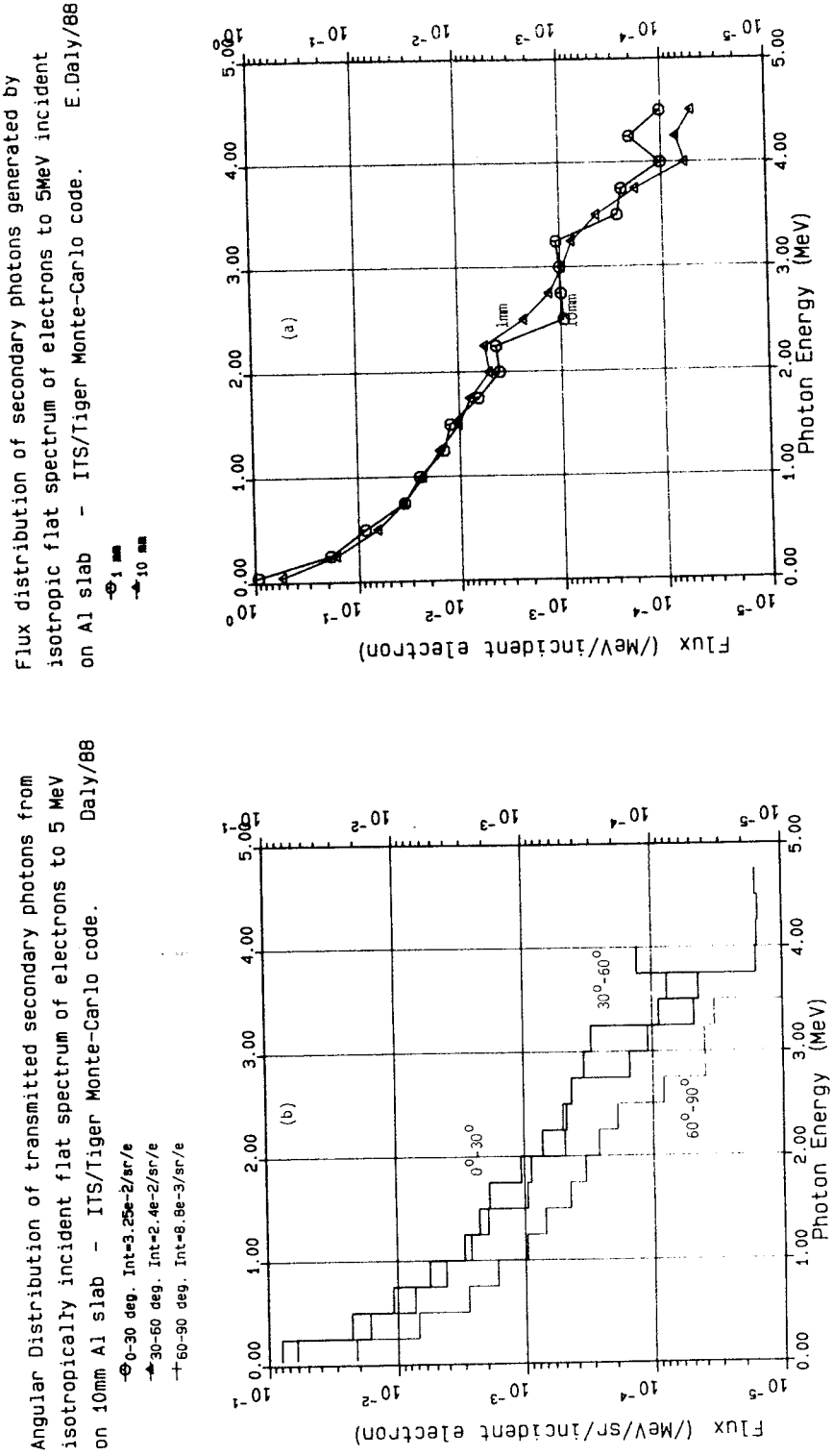

Bremsstrahlung spectra resulting from the flat electron spectrum of Figure 16.3. (a) shows spectra at 1mm and 10mm. The fluxes are differential in energy and normalised to unit incident current. (b) shows the transmitted spectra in three ranges of angles to the slab normal. These fluxes are differential in both energy and solid angle.

FIGURE 16.4

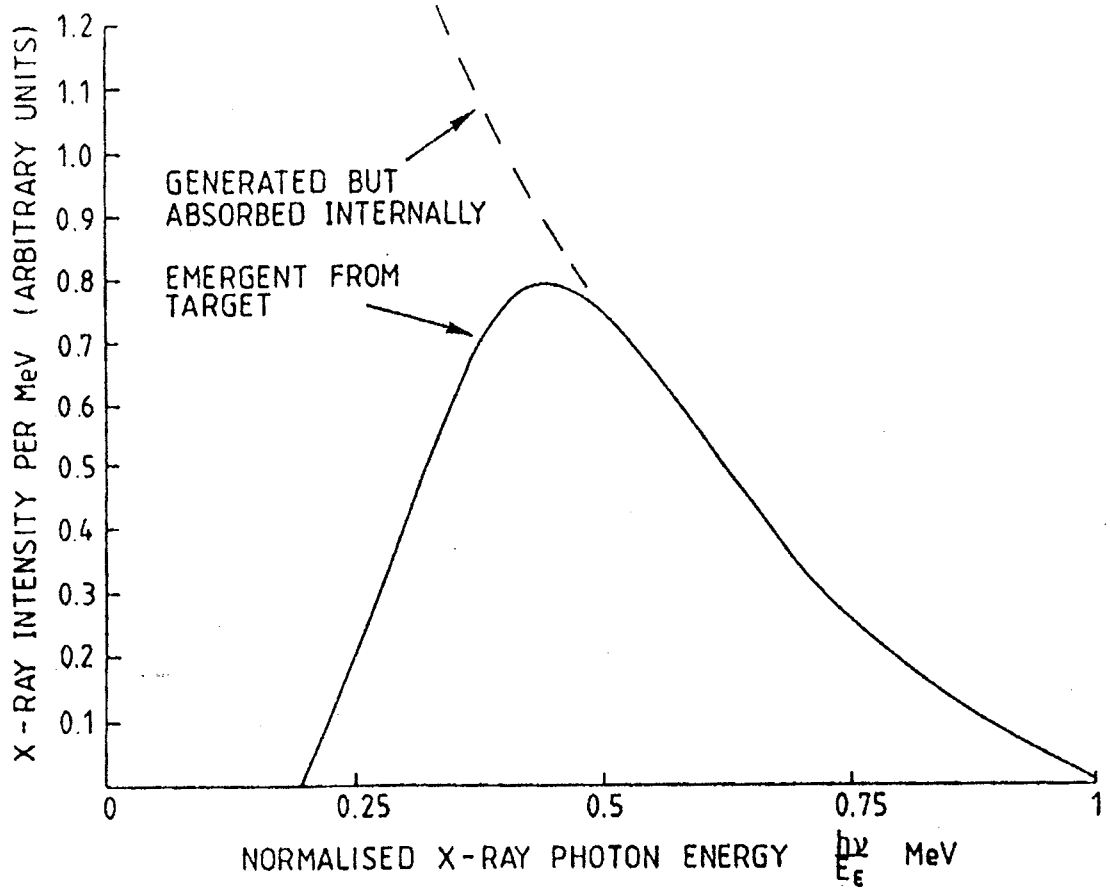

Spectrum of bremsstrahlung X-ray photons generated when electrons are slowed down in a material. For a 1 MeV electron, the energy scale can be read in MeV. The intensity expressed in rads integrated over the whole emergent spectrum will then be of the order of 10^{-12} rad(Si) per unit incident flux.

FIGURE 16.5 - GENERATION OF BREMSSTRAHLUNG

TABLE 16(1) - TYPICAL CHARACTERISTIC X-RAY EMISSION LINES FOR ELEMENTS OF IMPORTANCE IN SPACECRAFT AND DEVICES

Element	Atomic nr. (Z)	Highest 'K' line (keV)	Highest 'L' (keV)
Be	5	0.11	-
C	6	0.28	-
O	8	0.53	-
Al	13	1.56	0.07
Si	14	1.84	0.09
Ti	22	4.96	0.46
Cr	24	5.99	0.65
Mn	25	6.54	0.64
Fe	26	7.11	0.79
Co	27	7.71	0.79
Ni	28	8.33	0.94
Cu	29	8.98	1.02
Mo	42	20.00	2.51
Ta	73	67.42	11.67
W	74	69.48	12.10
Pt	78	78.34	13.56
Au	79	80.66	14.78
Tl	81	85.45	15.33
Pb	82	88.06	15.84
U	92	115.39	21.66

Adapted from R.C. Weast (Ed), "CRC Handbook of Chemistry and Physics" (CRC Company, Cleveland, Ohio, 1973).

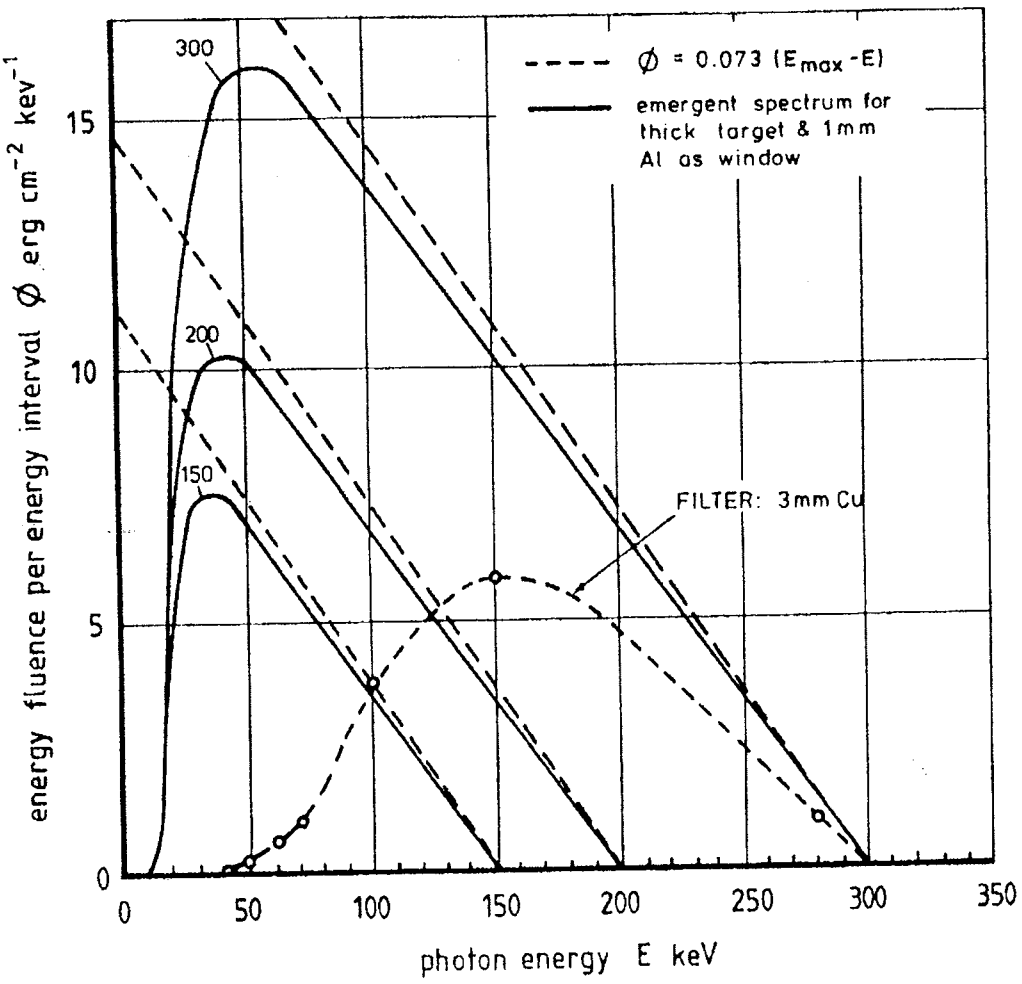

Ideal transmission of high-energy X-ray photons through plastic, aluminium and tungsten. No "build-up" included.

FIGURE 16.6 - BREMSSTRAHLUNG TRANSMISSION

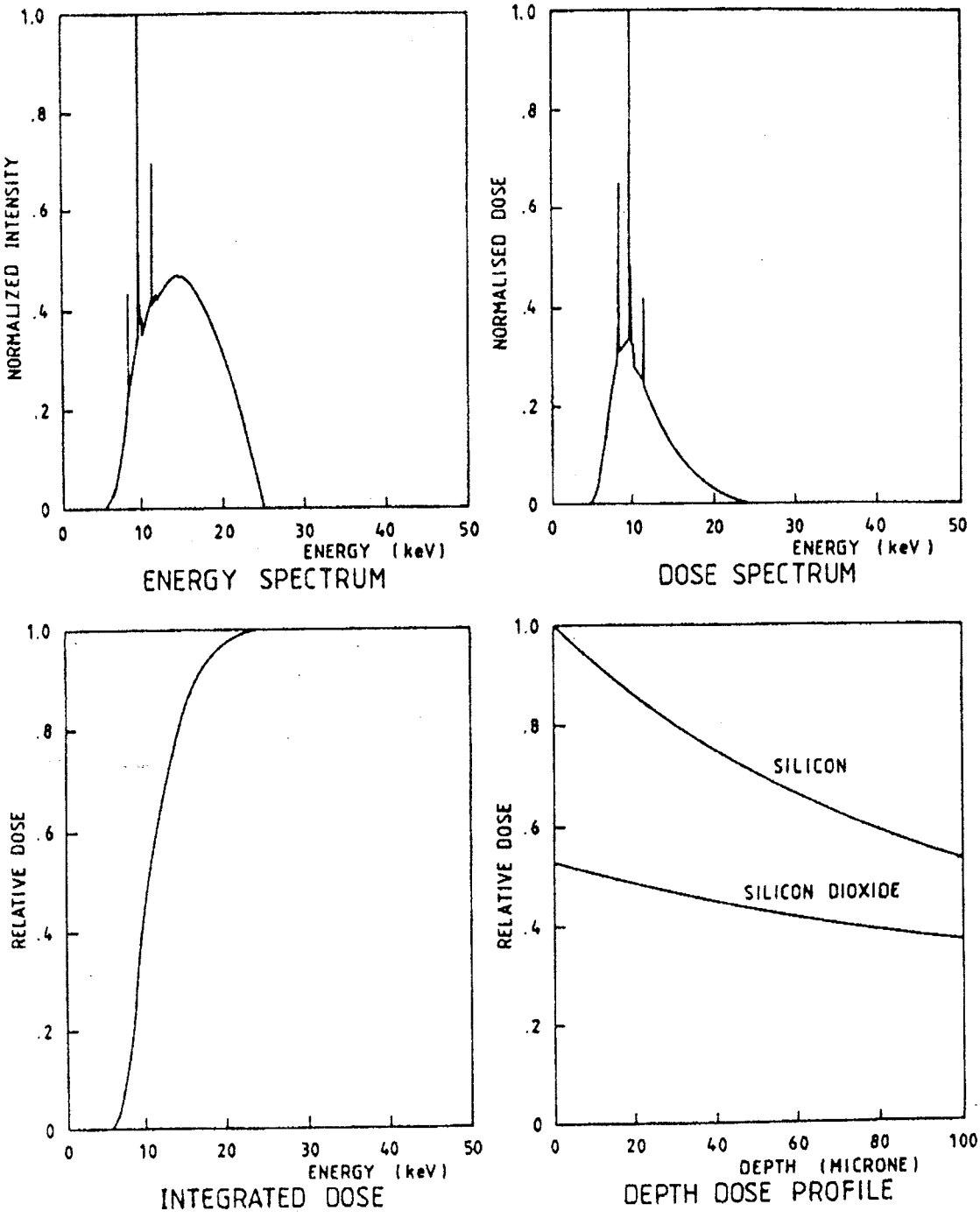

(Courtesy of Aracor Inc.)

FIGURE 16.7 - X-RAY ENERGY SPECTRA AND DOSES DEPOSITED BY A LOW-VOLTAGE MACHINE: 0.006" A.C. FILTER

16.4.4.2 Attenuation

An important feature of electromagnetic radiation in the 5 to 1000 keV range (X-rays) is the strong difference in attenuation from material to material and the very wide range of attenuation per unit thickness over that energy span. We will illustrate this with a few cases.

In ideal circumstances, known as "narrow geometry", X-rays are attenuated according to Lambert's Law:

$$I = I_0 e^{-\mu_m x_m} = I_0 e^{-\mu x} \qquad \text{.....16(iii)}$$

where $x_m = x$ is the areal density (thickness normalised to material density ρ, expressed in g/cm^2 or kg/m^2); μ is linear absorption coefficient and $\mu_m = \mu/\rho$ is the mass absorption coefficient.
μ is the attenuation coefficient for the material and is a total of the energy absorption and scattering powers of the constituent atoms.

μ is derived from the sum of all the interactions of a photon with a material (photoelectric absorption, Compton scattering etc.) and is often expressed in the form of a cross-section (a probability) of these interactions:

$$\sigma_{tot} = \sigma_1 + \sigma_2 \ldots \text{etc.} \qquad \text{.....16(iv)}$$

where σ tot is the total cross-section (probability) per atom and σ_1, σ_2 etc. are the probabilities for particular physical processes.

The relation of attenuation coefficient to the above is:

$$\mu = \frac{N_A Z}{A} \sigma \text{ for electron scattering} \qquad \text{.....16(v)}$$

The attenuation coefficient is sometimes given as the "mass attenuation coefficient" μ/ρ in units of $cm^2 . g^{-1}$.
For dosimetric calculations, another form of μ is used, namely the "energy absorption coefficient" which includes only radiation energy absorbed and ignores attenuation due to scattering.

A list of mass attenuation coefficients for megavolt photons is tabulated in Appendix D. The table shows that, in the region of 1MeV, the dependence of absorption upon atomic number is quite weak.

Thus, for example, 1 $gm.cm^{-2}$ of lead (0.1 mm) will produce 7% attenuation of 1 MeV photons while the same "mass thickness" of aluminium (3.7 mm) will produce 6%. Only large thicknesses of

aluminium (3.7 mm) will produce 6%. Only large thicknesses of shield material will significantly attenuate photons of these energies produced by Van Allen belt electrons.

It has been mentioned above that all materials are roughly equivalent in the efficiency of stopping X-rays in the megavolt range. Unfortunately, this statement ceases to hold at lower energies. At 100 keV, for instance, very great differences in absorption exist between, say, steel, plastic and biological materials. These differences are also tabulated in Appendix C. They greatly complicate testing with X-rays and make all dosimetry more complex. For example, the attenuation of X-rays at 5 keV is typically 10,000 times higher than at 1 MeV. This large factor implies that radiation testing procedures are less complex when high photon energies are used because package attenuation and scattering are less important.

16.4.4.3 "Build-up"

In calculating bremsstrahlung doses in spacecraft, it must be remembered that the "narrow geometry" required for the exact use of Lambert's Law does not hold. Higher doses will be obtained as a result of scattering effects, sometimes called "build-up", that increase the number of transmitted photons by a factor of 2 at all depths greater than about 5 mm.

Another effect of scattering is also referred to as "build-up"; in gamma radiation testing. "Build-up material" is placed around a sample to promote scattering equilibrium.

16.5 PROTONS AND OTHER HEAVY PARTICLES

16.5.1 Interactions

Energetic protons and ions, being heavier particles, are not subject to the high degree of scattering experienced by electrons and normally follow virtually straight paths. It is relatively easy to compute their slowing and energy deposition in materials and they have well-defined ranges.

There is a small, but not negligible, probability of protons and other ions interacting with atomic nuclei, causing fragmentation of the nucleus or emission of secondary neutrons and protons. Such fragments and secondaries are hazards which cannot be ignored in some circumstances, such as in manned missions or single-event processes. Secondary neutrons produced in spacecraft materials, or even the upper atmosphere, can again interact "inelastically" with nuclei, producing gamma-rays which may interfere with gamma-ray telescopes.

16.5.2 Energy loss and attenuation

The rate of ion energy loss is, as for electrons, defined by a "stopping power" formula (Berger and Seltzer, 1982):

$$\frac{dE}{dX} = \frac{4.\pi\, e^4\, z^2 \rho N_A Z}{m_0 v^2\, A} B_i \qquad \text{.....16(vi)}$$

where z is the ion charge number and Z is the material atomic number, B_i is the ion stopping number, N_A is Avogadro's number (6×10^{23}) and A the atomic mass number. $\rho N_A/A$ is the number of atoms per unit volume. Clearly, fully ionised energetic ions, such as cosmic rays, deposit energy very rapidly in a material and this gives rise to single-event phenomena (SEU, latchup and radiobiological damage). This energy loss expression can be readily evaluated to give particle ranges, residual energies and energy deposit, the latter relating to dose and upset.

16.6 RADIATION ATTENUATION BY SHIELDING AND DOSE-DEPOSITION IN TARGETS

16.6.1 Dose

Ionisation induced by the various particles described above on reaching a device results in damage as described in Section 5. Dose, the energy deposited per unit mass of material, is the basic parameter for evaluating ionisation-induced damage. More precisely, this is the "physical absorbed dose". The dose deposited in a "target" depends on the particle type and on the energy which it retains after passing though any surrounding material "shielding". The dose is simply computed from the product of the particle fluence at a particular point and the restricted stopping power of the particle. The qualifier "restricted" means that only the energy loss which results in *locally* deposited energy is considered; the generation of secondaries which travel some distance before depositing their energy is excluded (Berger and Seltzer, 1982).

Evaluation of biological effects of radiation normally involve the use of the quantity "dose equivalent". This quantity attempts to account for the differences in the effects of the same absorbed dose of different radiation types. It is related to absorbed dose by quality factors and dose modifying factors :

$$D_{bio} = \sum_{radiations} D_{phys} \,.\, Q(LET) \,.\, DMFs \qquad \text{.....16(vii)}$$

International standards exist for quality factors ; for electrons, X-and gamma-radiation, they are unity, whereas for ions they are a

function of particle stopping power (LET) and reach a value of 20. For fast neutrons, a value of 20 has been set by the ICRP.

There is some uncertainty attached to quality factors, dose modifying factors and to the applicability of the dose concept to heavy ions which have unique biological effects. There are a variety of biological effects over short and long time scales and at high and low dose rates (Bucker and Facius, 1988). This is clearly a highly complex field and beyond the scope of the present document.

16.6.2 Range

The range of a particle in a material is the thickness of material penetrated before the particle loses all its energy. "Practical range" (R_p) is the most probable range of a particle of a given incident energy. Some electrons, in particular, clearly penetrate thicknesses greater than R_p and are often termed "straggling electrons". The term "maximum range" takes this into account ; the distinction will be illustrated more clearly in the subsequent discussion of transmission coefficients.

Range may be expressed either in units of depth (length) or, more commonly, as the product of depth and density ($g.cm^{-2}$). This unit is equivalent to mass per unit area and is used frequently in radiation studies as a measure of absorber thickness (may be termed "shield thickness" in some diagrams). For convenience, we shall henceforward refer to this unit as "mass thickness". Some range values for electrons and proton ranges in aluminium are tabulated in an appendix to this document.

The range of a particle at a given incidence particle energy, when expressed in $g.cm^{-2}$, is closely similar for all materials. There are second-order effects dependent on excitation potential and atomic number, but - at the energies likely to be encountered in the space environment - the spread in range is no more than a factor of two. Plots of the practical ranges of electrons and protons in a number of materials are shown in Figure 16.8. The data of both particles in Si is taken from Berger and Seltzer (1964 and 1966) and from Barkas and Berger (1964). Ranges in aluminium are given by Linnenbom (1962) and proton ranges in aluminium are also given by Cooley and Janda (1963). Data of electron and proton range in various other materials, including germanium and liquid propane, are also given by Berger and Seltzer (1971). When expressed in $g.cm^{-2}$, these ranges are almost coincident with those shown in Figure 16.8 and have therefore been omitted for the sake of clarity.

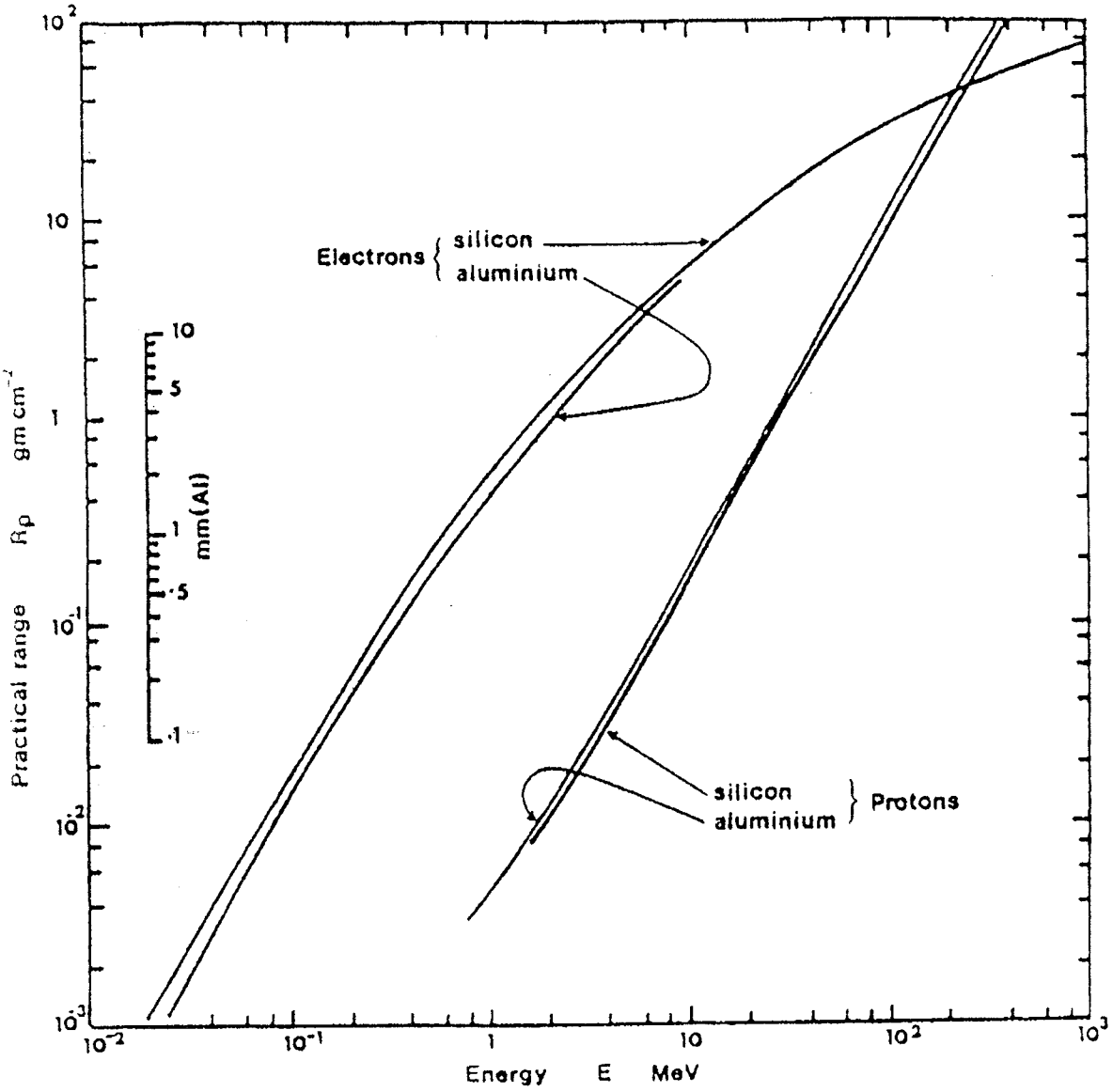

The range of electrons and protons in aluminium and silicon as a function of incident energy.

FIGURE 16.8 - PARTICLE RANGE IN MATERIALS

16.6.3 Relationship between incident flux and deposited dose

In performing evaluations of radiation environments, it is often most convenient to consider a silicon target shielded by aluminium since this relates closely to typical electronic devices in spacecraft and is the basis for much testing work and calculation. The effect of shielding is generally to reduce fluxes of primary particles, to lead to creation and subsequent absorption of secondary radiations and to change the energy spectra of the radiation. Therefore the dose in a target depends on the amount of shielding in a way that is not simple to calculate.

For engineering purposes, a "dose-depth" curve is often used to represent the space radiation environment, its modification by shielding and the resulting dose in components. This gives the dose, either for the individual components of the environment (protons, electrons, bremsstrahlung etc) or the sum of the components, as a function of the thickness of shielding material, usually aluminium. This removes all information about particle energies or even particle type and is usually an integration over orbits or complete missions.

This subsection provides data with which the dose in silicon can be calculated for various thicknesses of aluminium shielding. Computer programs for such purposes are readily available and readers who have a continuing need for such calculations are advised to obtain copies of these programs. Section 18 contains details on programs and how to obtain them.

We will now consider how to calculate the dose which is produced behind a given thickness of aluminium shielding by electrons, electron-induced bremsstrahlung and protons resulting from the broad spectra of electrons and protons found in space.

Seltzer (1979) used the ETRAN Monte-Carlo computer code, simulating the propagation of electrons and photons (bremsstrahlung), to compute the dose generated at different depths in planar, semi-infinite (one-dimensional) aluminium shielding for a range of incident *isotropic, monoenergetic* electron energies. The d(x,E) data set thus created allows an arbitrary input spectrum f(E) to be folded with d(x,E) to yield a sum dose at depth x due to the spectrum. This is normally done by the SHIELDOSE computer program, but can be done manually, given the data. In addition to electrons and bremsstrahlung, Seltzer's data set includes doses from protons, computed by means of the straight-ahead, continuous-slowing-down approximation.

The data set is organised in normalised form, with the depth scale normalised with range and the doses energy-, range- and current-normalised and made dimensionless.

For each type of use, these have been converted to dose (Si) per unit incident isotropic (4 π) electron or proton flux and are shown in Figures 16.9-16.11. There is a pair of curves for each of the important radiation types; electrons, electron-induced bremsstrahlung and protons. For each type, the curves (a) give the doses as functions of incident particle energy for various shielding depths while the curves (b) give the doses as functions of shield depth for various incident particle energies.

In performing an evaluation of the expected radiation dose on a space mission, the shielding geometry should be given some thought. It should be recognized that the doses provided in these figures are for a *planar shield* where, clearly, radiation comes principally from one side and paths which are not normal to the face encounter increased amounts of shielding.

The popularity of planar and slab geometries arises from the efficiency with which Monte-Carlo analyses can be performed with them. A less optimistic basis for the evaluation of shielding effects is to assume spherical shielding. When the dose point is located at the centre, minimum shielding is encountered in all directions. This is preferable for initial evaluation except where there is good justification for the assumption of planar shielding, for example when considering surface materials.

Dose at the centre of a solid sphere of radius z can be derived from the planar dose at depth z by means of the approximation (Seltzer, 1979):

$$D_{sp}(z) = 2D_{pl}(z) \cdot \left(1 - \frac{d\ \log(D)}{d\ \log(z)}\right) \qquad \text{.....16(viii)}$$

If solid-angle sectoring is employed for analysis of complex geometries, doses based on spherical shielding should be used.

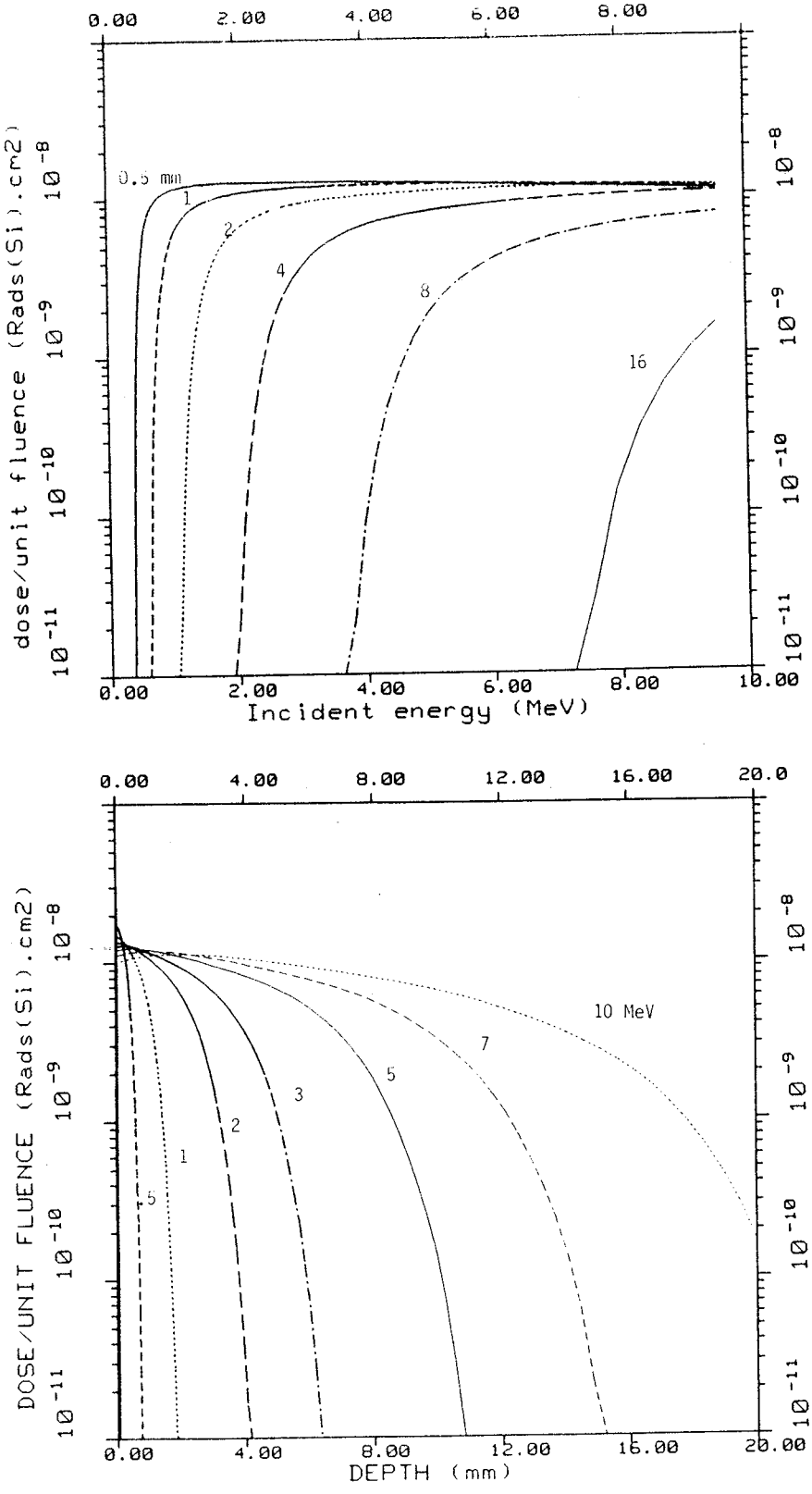

Electron dose deposition in planar semi-infinite aluminium shielding (a) as functions of incident electron energy for different shield depths (mm) and (b) as functions of shield depth for different incident electron energies (MeV). Dose is for silicon and is normalised to unit incident isotropic flux.

FIGURE 16.9

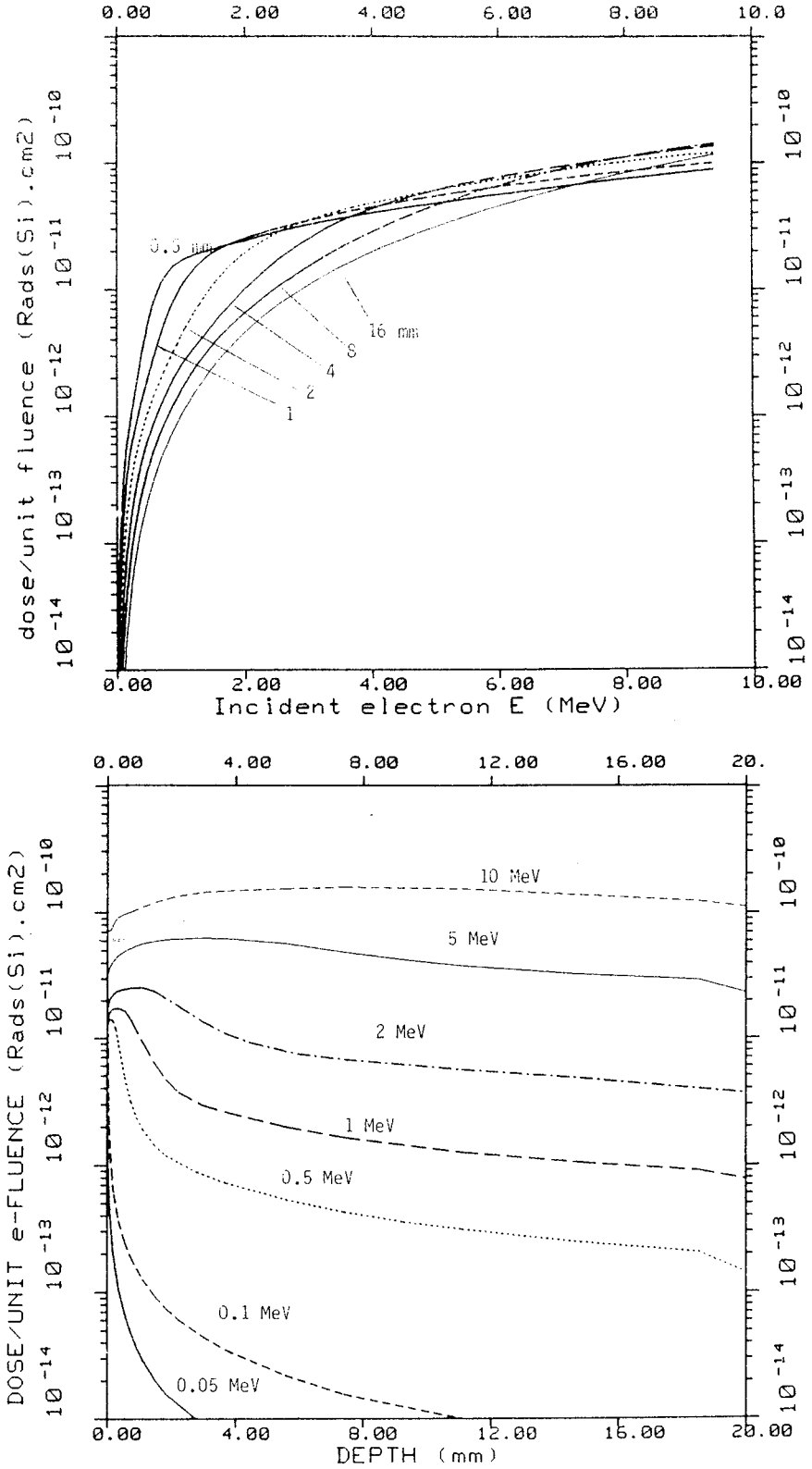

Bremsstrahlung dose deposition in planar semi-infinite aluminium shielding (a) as functions of incident electron energy for different shield depths (mm) and (b) as functions of shield depth for different incident electron energies (MeV). Dose is for silicon and is normalised to unit incident isotropic electron flux.

FIGURE 16.10

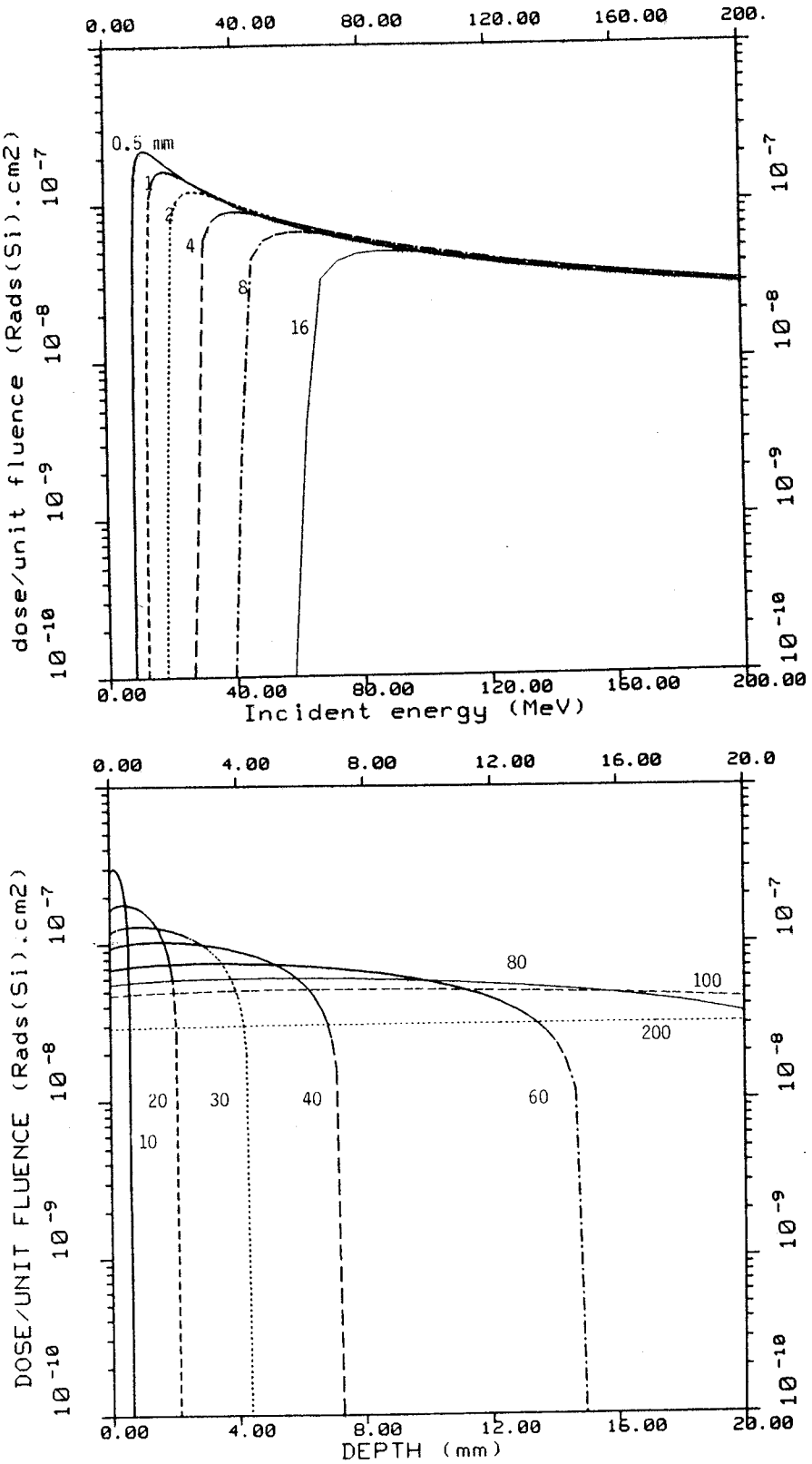

Proton dose deposition in planar semi-infinite aluminium shielding (a) as functions of incident proton energy for different shield depths (mm) and (b) as functions of shield depth for different incident proton energies (MeV). Dose is for silicon and is normalised to unit incident isotropic flux.

FIGURE 16.11

16.6.4 Dose calculation procedure

It is now possible to calculate the relationship between ionisation dose and the depth of absorber (for the time being, only the special case of silicon shielded by aluminium is considered) for any spacecraft orbit where the integrated flux vs energy spectrum is known. The calculation is performed by combining the particle spectrum with the relevant dose transmission curves (Figures 16.9 to 16.11). In principle, the procedure described below is identical for electrons, electron-induced bremsstrahlung and protons.

Given:

(a) Spectrum of omnidirectional integral flux, ϕ (>E) versus energy E,

(b) Dose per unit fluence curves, D_F (d), showing dose per unit particle fluence versus incident energy at a specified depth (or "mass thickness").

Procedure:

(i) Calculate flux element in a small energy interval of width ΔE and of mean energy E_m .

$$\Delta\phi(E_m) = \phi(>E_1) - \phi(>E_2) \qquad \text{.....16(ix)}$$

where

$$E_1 - E_2 = \Delta E$$

Alternatively, if differential spectra are available:

$$\Delta\phi(E_m) = \frac{d\phi(E_m)}{dE} \times \Delta E \qquad \text{.....16(x)}$$

(ii) Read the dose per unit fluence, D_F (d), at energy E_m for the appropriate absorber thickness d.

Calculate the dose contribution ΔD (per unit time) due to the flux element in energy interval:.

$$\Delta D(dE_m) = D_F(d,E_m) \times \Delta\phi(E_m) \qquad \text{.....16(xi)}$$

Note here that multiplication of the dose per unit fluence by the flux (fluence per unit time) yields, strictly, a dose rate. The time unit for dose rate is often given as the mission duration (e.g. 7 years); in this context, the term "total dose" is often used to describe mission dose.

(iii) Calculate the total dose for thickness d by adding dose contributions from the energy intervals covering the whole energy spectrum.

Thus, the total dose $D(d) = \sum_{E_m} \Delta D(d,E_m)$ at all E.

(iv) Repeat the procedure for several values of thickness d. Plot D(d) against d, giving the "Dose-depth" curve.

(v) Repeat the procedure for each component of the environment, trapped protons and electrons, and solar flare protons. Note that for calculating the bremsstrahlung dose, the electron flux is used together with the bremsstrahlung dose data.

We are free to choose the width of the "small" energy intervals and of the energy spectrum over which to collect dose contributions. Clearly, more accurate results are obtained by considering larger numbers of energy intervals of smaller width.

The "hardness" of the flux spectrum, dependent upon the rate of change of flux with energy, is an important factor in the actual choice (a "hard" spectrum is one showing little change with energy). As far as the spectrum width is concerned, it is clear that the lower limit is set by the thickness (and therefore particle range) being considered. The higher limit is effectively reached when dose contributions from successive energy intervals cease to be a significant part of the total. Thus, for non-computerised calculations, a certain degree of trial and error is necessary.

16.7 ATOMIC DISPLACEMENT DAMAGE

The degradation of energy and number of particles as they proceed through a slab of absorber has been explained in detail in preceding sections dealing with the ionisation dose versus depth relations for absorbers surrounding electronic equipment. Curves analogous to those for dose transmission may sometimes be required for a limited range of electronic devices which are also sensitive to displacement damage. Thus, in the same way as before, generalised damage tramsmission versus energy curves may be made first so that "damage-depth" curves can be calculated for a given set of particle spectra. Brown, Gabbe and Rosenzweig constructed such curves on the same general basis as our dose transmission shown here as Figures 16.12 and 16.13. They are useful in, for instance, studies of solar cells.

For a complete description of solar cell degradation and the concept of damage equivalence for evaluating such degradation, the reader is referred to Tada et el. (1982). They also give, for a variety of solar cells, the degradation to be expected in cell output

Data handling equipment employs high-speed bipolar transistors which are insensitive to the displacement effect by virtue of their design.

The narrow base region confers this insensitivity (see Section 7). Some power transistors have base regions wide enough to experience damage-induced gain degradation, but the use of these in the power units of a spacecraft can usually be avoided. Finally, an order of magnitude calculation shows that, except for the very inhospitable inner-belt "heart" region, vehicles in 5-year circular equatorial orbits will not experience sufficient exposure for serious damage to occur in transistors of medium-power design (frequency cut-off about 100 MHz). "Serious damage" here may be taken to represent a decrease of 10% in gain. For dealing with such transistors, or even more sensitive ones of wider base (lower frequency cut-off), the "BGR" damage curves will suffice so long as the vertical scale is multiplied by 2 to allow for non-infinite back-shielding. It should be noted that in typical fast-switching transistors in space, the "surface effect" due to ionisation will be more problematical than the atomic displacement effect.

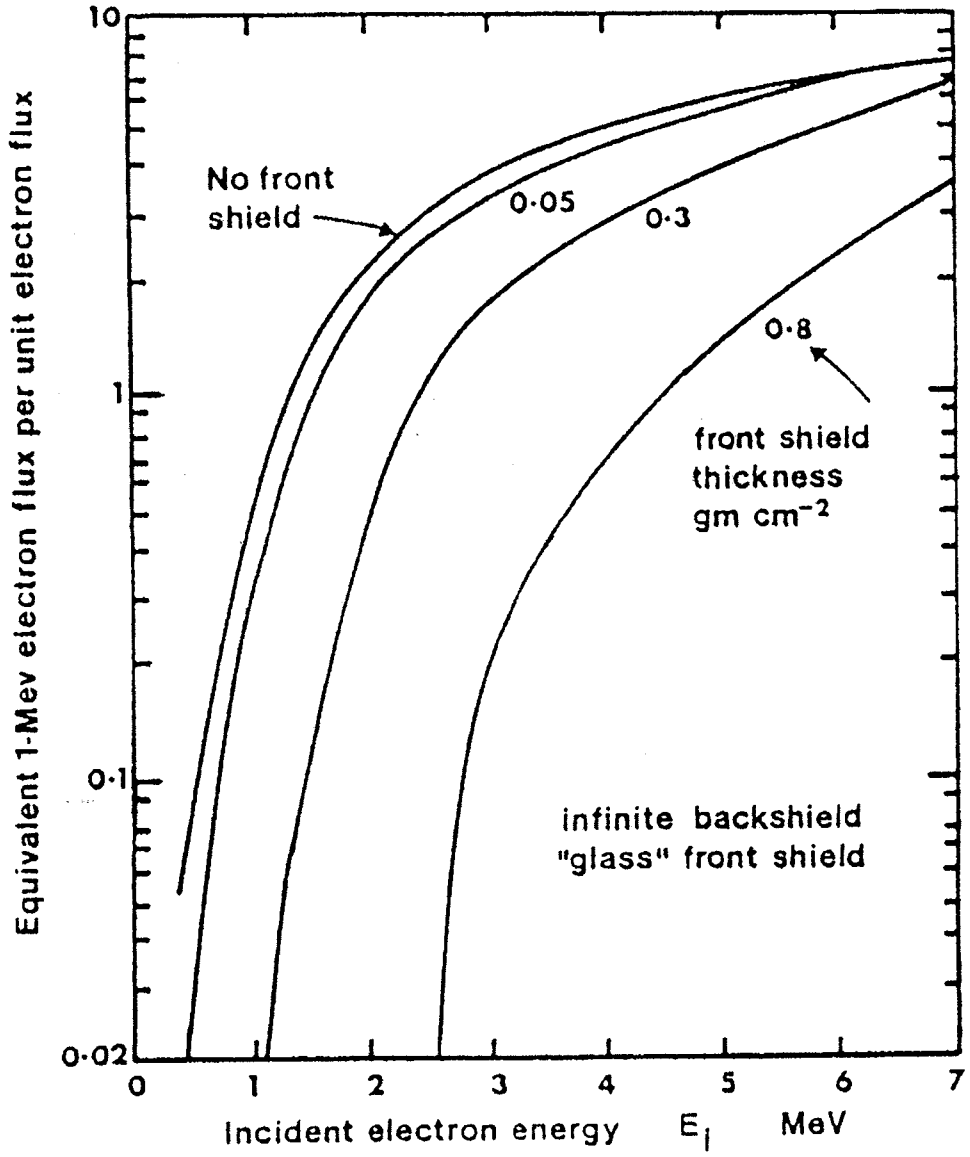

The "BGR" damage transmission curves, giving the damage-equivalent 1-MeV electron flux as a function of the energy of a monoenergetic isotropic flux of electrons incident upon n-on-p solar cells with various front shielding. The back-shield is assumed to be infinitely thick. For uniform all-round shielding, the vertical scale should be multiplied by two. The front-shielding would be a typical solar-cell cover glass.

FIGURE 16.12 - ELECTON DAMAGE TRANSMISSION

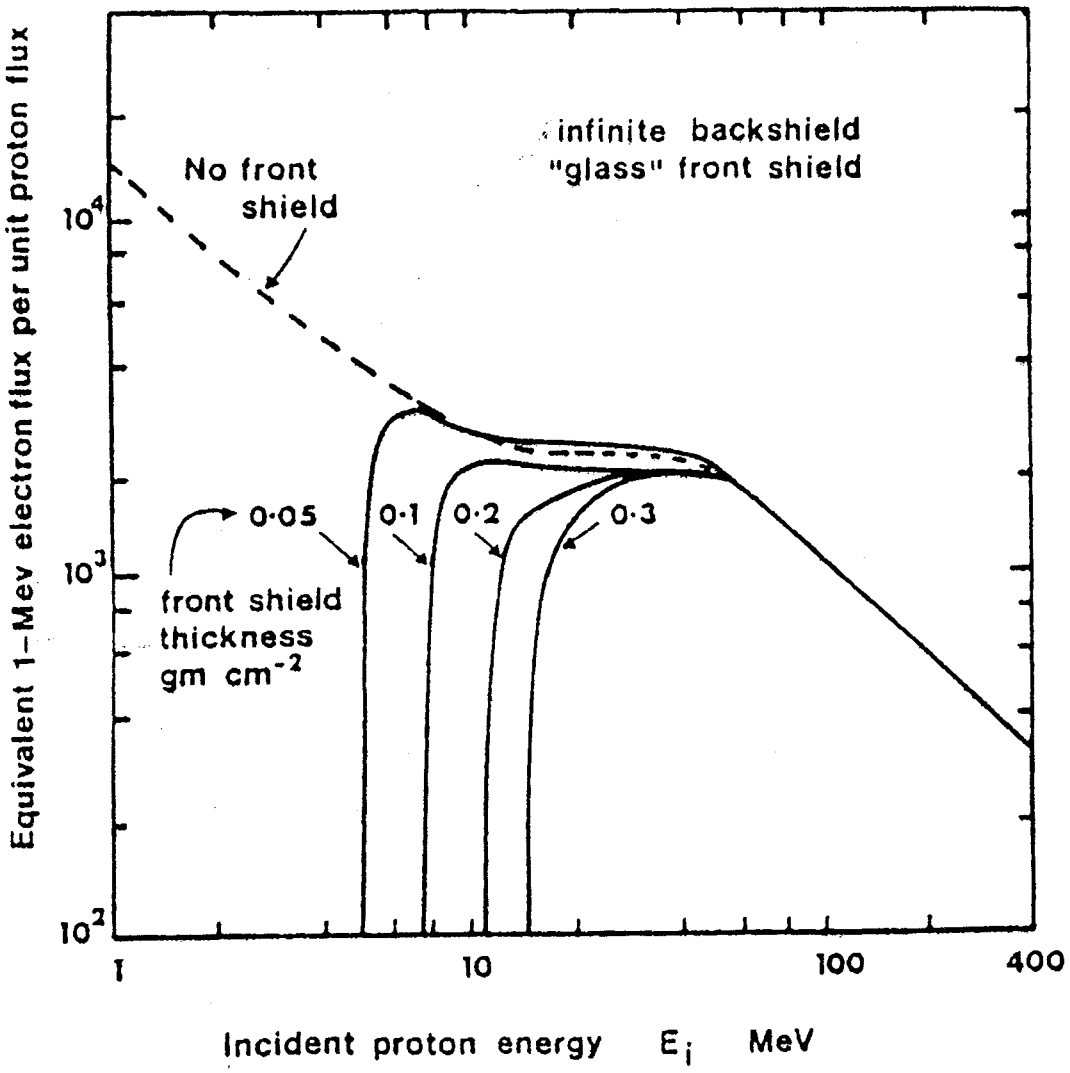

The "BGR" damage transmission curves, giving the damage-equivalent 1-MeV electron flux as a function of the energy of a monoenergetic isotropic flux of protrons incident upon n-on-p solar cells with various front shielding. The back-shield is assumed to be infinitely thick. For uniform all-round shielding, the vertical scale should be multiplied by two. The front-shielding would be a typical solar-cell cover glass.

FIGURE 16.13 - PROTON DAMAGE TRANSMISSION

16.8 MATERIAL EFFECTS

16.8.1. Deposition of dose

The procedure for deriving the dose-depth curves described in the preceding sections has been applied to the typical case of a silicon device protected by an aluminium absorber. To estimate doses deposited in materials other than silicon, the appropriate "stopping power" data should strictly be used as the basis of the dose per unit fluence calculation. In practice, however, stopping power (when expressed in "mass thickness" units) does not vary greatly from material to material.

Figures 16.14 and 16.15 show electron and proton stopping powers for various materials normalised, for convenience, to the values for aluminium. Stopping power values for silica, for instance, are not available, but it is reasonable to assume that they are no more than a few percent greater than those for silicon. Clearly, it would be essential to make the appropriate corrections when calculating the dose in materials such as water (human tissue), polyethylene or heavy materials such as gold, where stopping power values are further removed from those of silicon or aluminium.

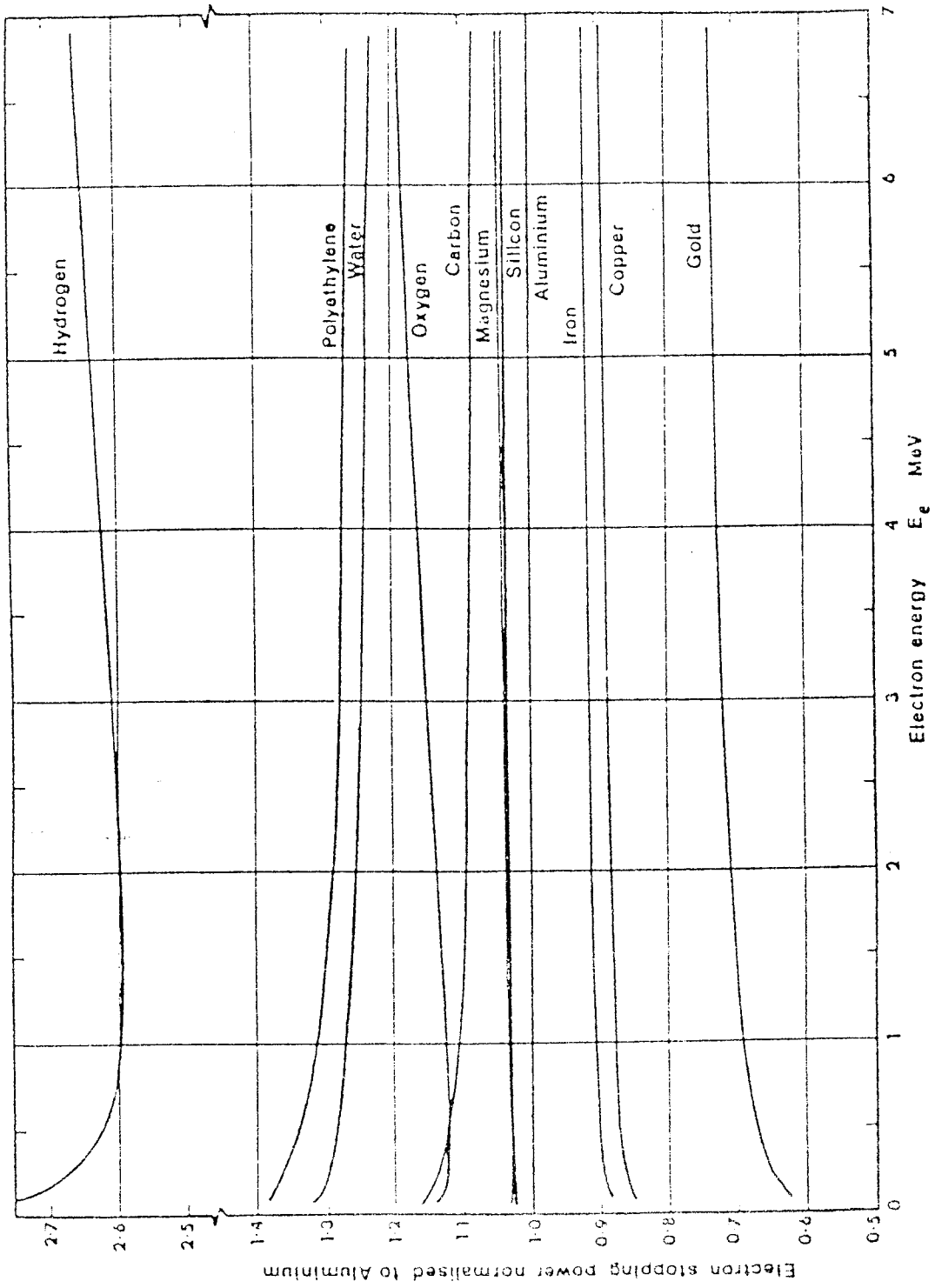

The electron stopping power for various materials, normalised against aluminium, as a function of incident energy.

FIGURE 16.14 - ELECTRON STOPPING POWER; EFFECT OF DIFFERENT MATERIALS

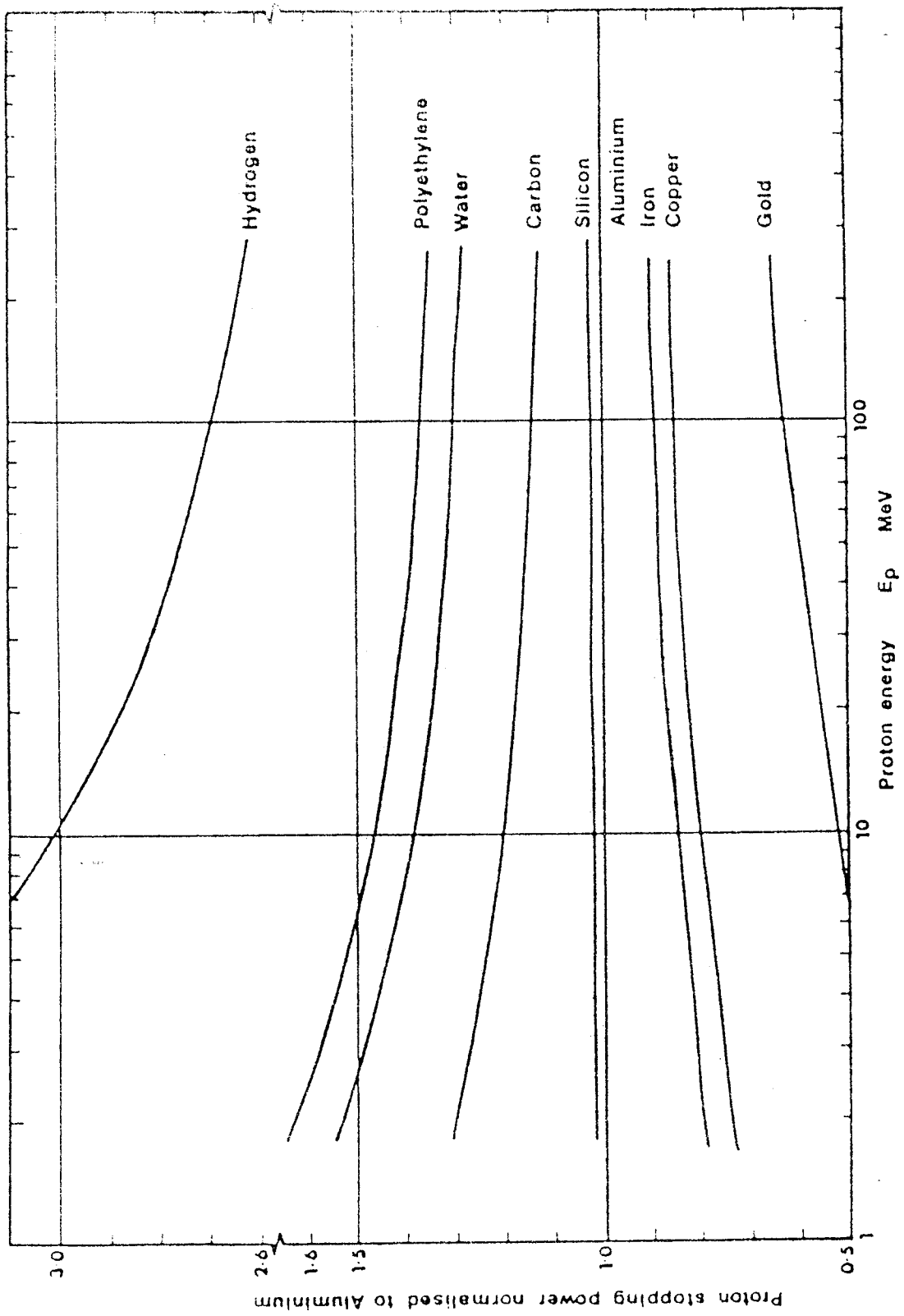

The proton stopping power for various materials, normalised against aluminium, as a function of incident energy.

FIGURE 16.15 - PROTON STOPPING POWER; EFFECT OF DIFFERENT MATERIALS

16.8.2. Other shielding materials

For the calculation of radiation doses behind different absorbing or shield materials, it has often been practice "to convert" all materials to equivalent aluminium thickness by making the appropriate density correction. The use of an alumium dose-depth curve for all materials thus requires the assumption that transmission coefficients for a given "mass thickness" will be the same for any material. This may lead to considerable error, especially in the case of electron doses.

In certain circumstances, and especially in orbits such as geostationary where electron and bremsstrahlung doses dominate, the reduction of all materials to "aluminium equivalent" can lead to significant error. Evaluation based on aluminium equivalents is useful for initial analysis to identify potential problem areas. A more rigorous analysis which may subsequently be required should account for the different materials, possibly by application of the computer programs described in Section 18 to "multi-layer structures".

The need for the multilayer approach arises from the strong degree of scattering of electrons by matter and the strong dependence of this effect on atomic number. As a result, a slab of material of high atomic number transmits fewer electrons than one of low atomic number with the same "mass thickness". Figure 16.16 shows this effect for several different materials (Mar, 1966). The electrons are scattered out of the transmitted beam; many, in fact, in a backward direction. Figure 16.17, based on data from Wright and Trump (1962) shows experimental results for the back-scattering of megavolt electrons from thick targets. It will be seen that lead is 5 to 10 times more efficient at back-scattering than aluminium. It is not surprising, therefore, that the opposite, but far weaker dependence of electron "stopping power" on atomic weight is swamped by the scattering effects.

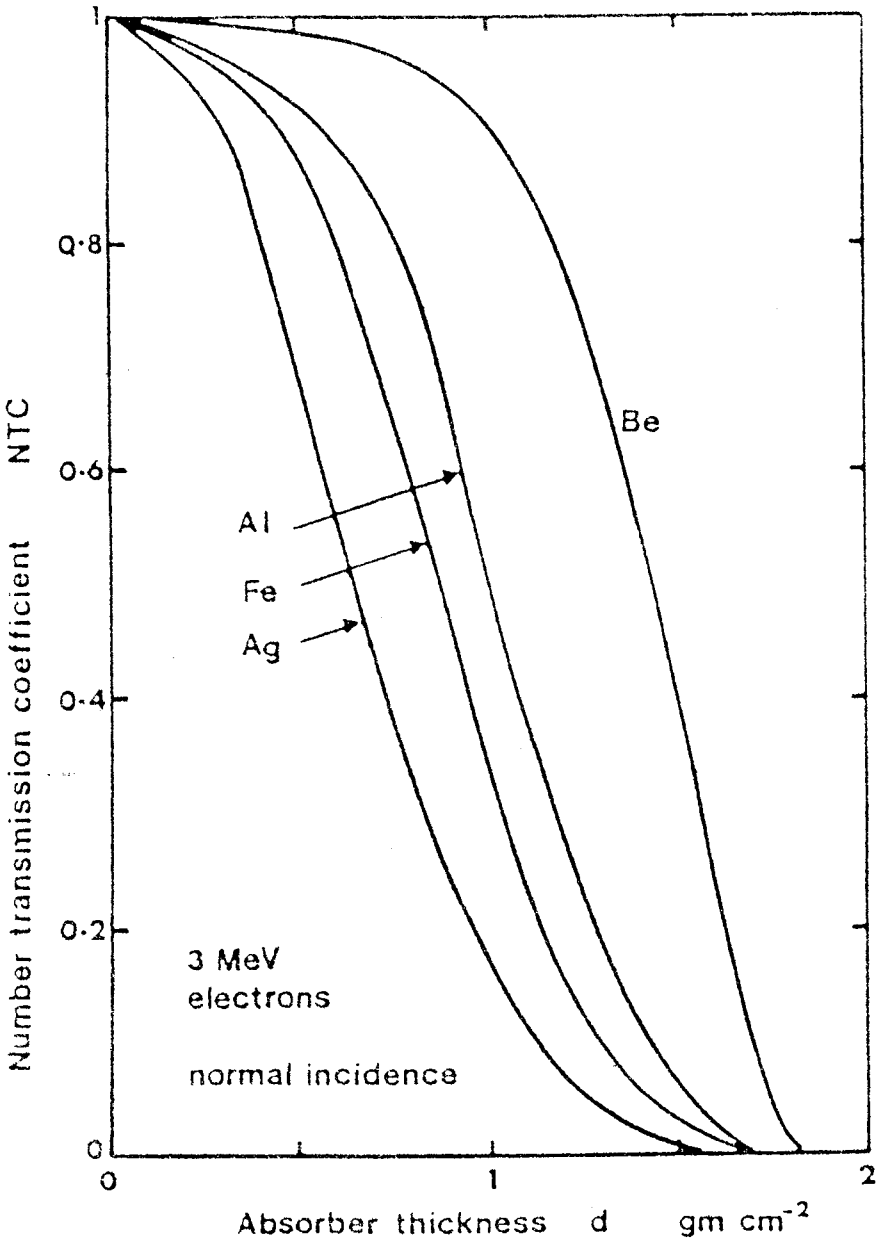

Number transmission coefficient for 3 MeV electrons as a function of absorber thickness for several absorber materials.

FIGURE 16.16 - ELECTRON TRANSMISSION; EFFECT OF DIFFERENT MATERIALS

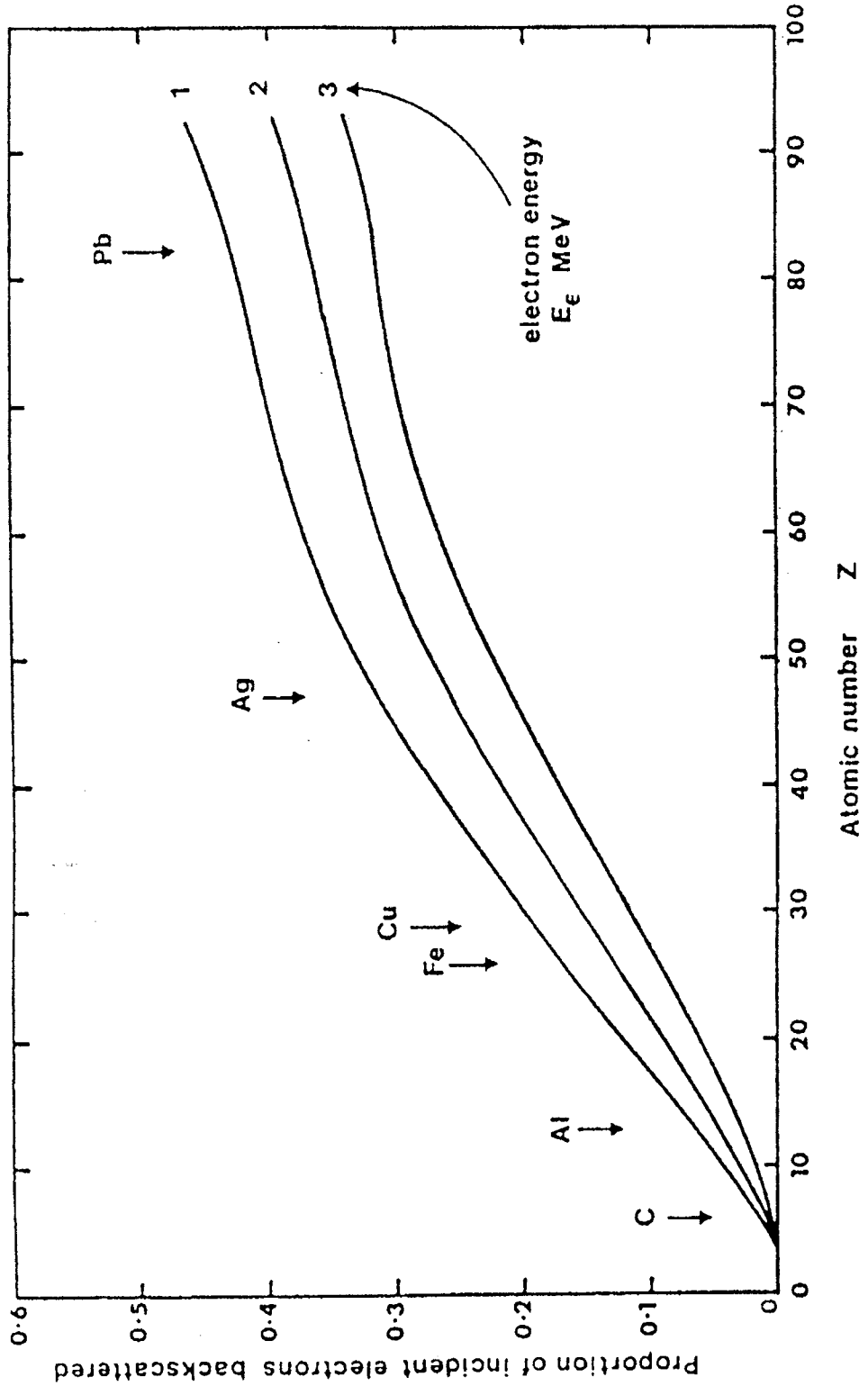

The fractional backscattering of electrons as a function of atomic number of absorber material.

FIGURE 16.17 - ELECTRON BACK SCATTERING

As an illustration of the effect of heavier shielding material on back scattering and bremsstrahlung generation, Figure 16.18 shows dose-depth curves (for electron and bremsstrahlung doses) for equivalent mass-thicknesses of aluminium and lead absorbers in the geostationary orbit environment. It can be seen that, for shield thicknesses less than 1 $g.cm^{-2}$, lead is a more efficient absorber. However, this degree of protection will be satisfactory only for devices that tolerate total doses of greater than 10^4 rad(Si) over a 7-year mission. For more sensitive devices requiring greater protection, the bremsstrahlung generated by lead is likely to provide an irreducible and unacceptable background. The same strong dependence on atomic weight does not hold for protons on account of their greater mass.

These curves are derived from old electron models and an approximate dose calculation and are intended only to demonstrate a trend and should not be used directly in generating design rules. They represent the artificial, simplified case of a uniform absorber of a single material.

If we consider the case of a composite absorber consisting of, say, lead and aluminium layers, then the composite dose-depth relationship would clearly be expected to lie somewhere between the extremes of lead and aluminium, and would depend upon the proportion of the overall mass-thickness contributed by each material. It must be remembered, however, that most of the bremsstrahlung is generated in the outermost part of the absorber where the lower-energy electrons are stopped. Therefore, the effect of adding lead to the outside of aluminium shielding would be to limit the minimum dose to something close to the lead bremsstrahlung level. If, on the other hand, lead were the innermost component of the composite, the two advantages of the better electron shielding of the lead and the lower bremsstrahlung generation in the aluminium could, in principle, be combined. In practice, a large amount of absorber will often consist of epoxy-glass laminate (see Appendix C) with transmission coefficients lying between the values for carbon and aluminium.

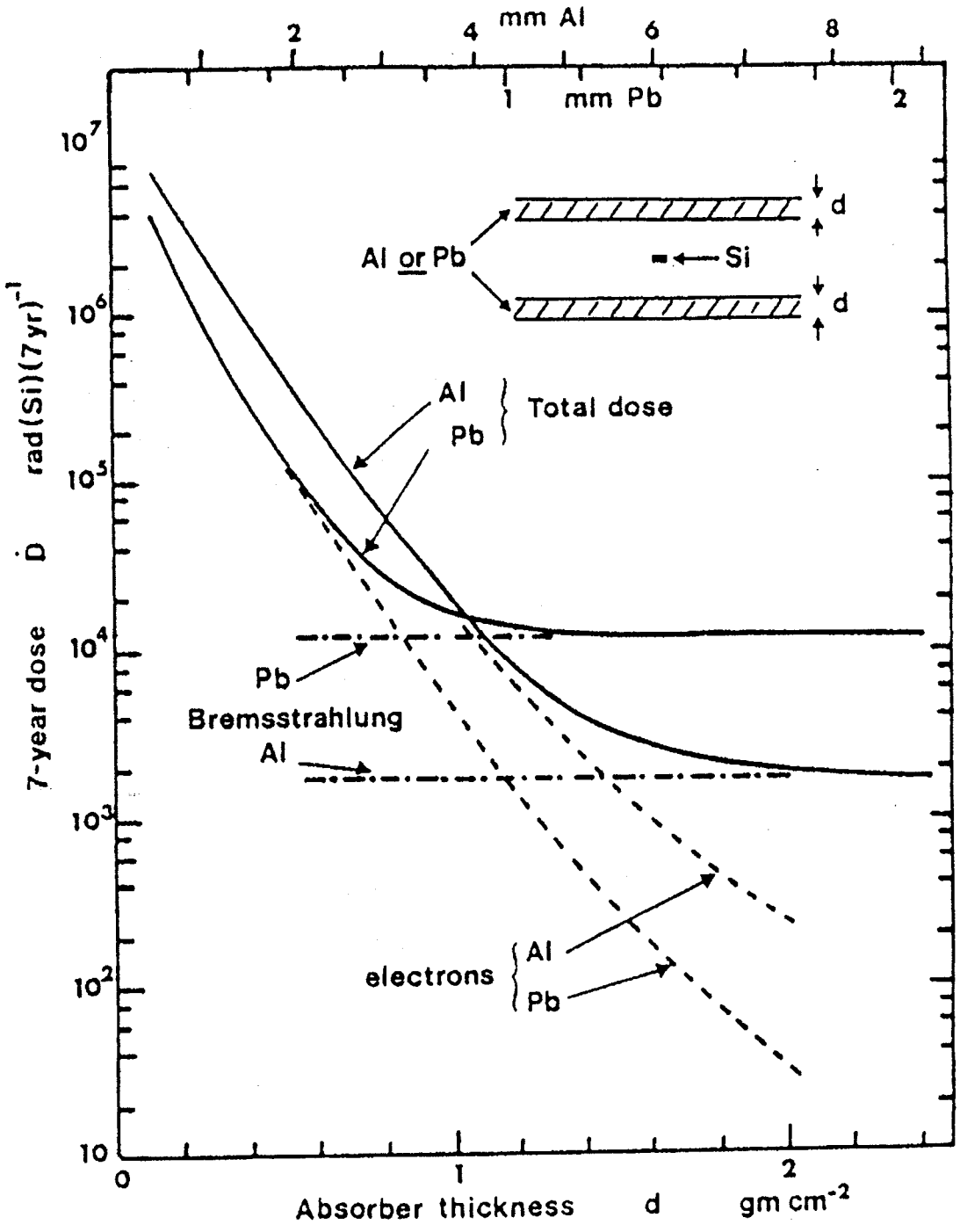

Dose-depth curves for the geostationary orbit showing the effect of different absorber materials. The curve for lead absorber is a provisional estimate.

FIGURE 16.18 - DOSE-DEPTH CURVES; EFFECT ON DIFFERENT ABSORBER MATERIALS

Using Monte Carlo calculation methods, Mar (1966) has made a study of electron transmission as a function of atomic number and derived complex expressions for number transmission coefficient and transmitted flux/energy distribution for monoenergetic incident electrons.

$$NTC(E,Z,X) = \exp\left\{ -\left(\frac{0.634\ EZ^{0.23}}{X^{0.848}} \right)^{-K} \right\} \qquad \text{.....16(xii)}$$

where $k = 7(Z-3.25)^{-0.24}$ and where E, Z and X are incident electron energy, atomic number and shield thickness respectively. The transmitted differential flux distribution is represented by the expression

$$\phi(E_e, Z, X)dE = A\,[\exp[-b(E - E_e)]]\,dE,$$

where

E_e = emergent electron energy,
A = a constant,
$b = (X/E)^{-1.46}(1.53 - 0.0147\ Z)/E$.

A boundary condition, $\phi dE = 0$ for $E_e > E_{max}$, applies to this formula, where E_{max} is the peak or "most probable" transmitted energy. This expression reflects therefore the finite width of the emergent energy spectrum after transmission of a monoenergetic incident flux (see Section 16.3).

Mar's approximation in this case is to consider the transmitted spectrum as a vertical edge (E_{max}) with an exponentially decaying distribution at energy less than E_{max}. This is in order except that as shield thickness increases, the transmitted energy spectrum becomes broader and the vertical-edge approximation less appropriate.

16.8.3. Routine calculation of particle transmission

It has been demonstrated that because of heavy scattering effects, electron transmission in different materials is extremely variable. Merely to use "stopping powers" and Number Transmission Coefficients (NTC) in estimating shielding effects can lead to errors. This is best achieved through computer calculation. The calculation of bremsstrahlung is also highly complex and best performed by computer. Section 18 gives details of suitable computer codes.

16.9 ORBITAL DOSE AND DAMAGE DATA

16.9.1. Orbital dose-depth curves

In the preceding subsections, the interactions of radiation with matter, shielding and resultant dose and damage caused by the radiation were discussed. Section 3 described the radiation environment external to the spacecraft, in terms of particle fluxes and showed how environment models could be used to provide "orbital integrations" which describe the environment in terms of orbit-average particle flux-vs-energy spectra. Using the data presented in Subsection 16.6, these orbital environments can be translated into dose behind given amounts of shielding. In fact, the SHIELDOSE program has been used to do this automatically.

Figures 16.19 and 16.20 show typical results of the process: the orbital dose-depth curves. These show the annual doses expected in Low Earth Orbit (LEO) at solar minimum and in geostationary orbit at solar maximum as functions of spherical aluminium shield thickness. The contributions of the various radiation species to the total doses are also shown. These represent very different regimes of the radiation environment.

LEO orbits encounter very energetic radiation-belt protons, but a "soft" electron environment and therefore relatively low bremsstrahlung doses. Solar flare particles cannot penetrate to LEO orbits because of geomagnetic shielding (see Section 3). The proton dose becomes very flat with shields more than about 4 mm thick and clearly the effectiveness of additional shielding is then poor.

Geostationary orbits are beyond the proton radiation belt, but are exposed to quite a severe electron environment. This results in much higher doses than in LEO for shield thicknesses below 6 mm, before the electrons become attenuated. The electrons generate bremsstrahlung which is not so easily attenuated, resulting in a slowly decreasing dose as the shielding is increased. Also shown are doses expected from energetic protons from a single anomalously large solar flare event. Care should be taken not to scale this contribution with time since such events are infrequent. The flatness of the bremsstrahlung and solar proton dose-depth curves means that, as in LEO, the efficiency of additional shielding for shields thicker than about 7 mm is low, although the causes are different in the two cases. To affect such bremsstrahlung doses significantly would require the use of high-Z shielding materials.

Annex F contains a full selection of dose-depth curves for various orbits. These show that other orbits are generally a combination of the two cases presented above. Elliptical orbits and polar orbits, for example, encounter inner-zone protons and outer-zone electrons and are partially exposed to particles from solar-flare events.

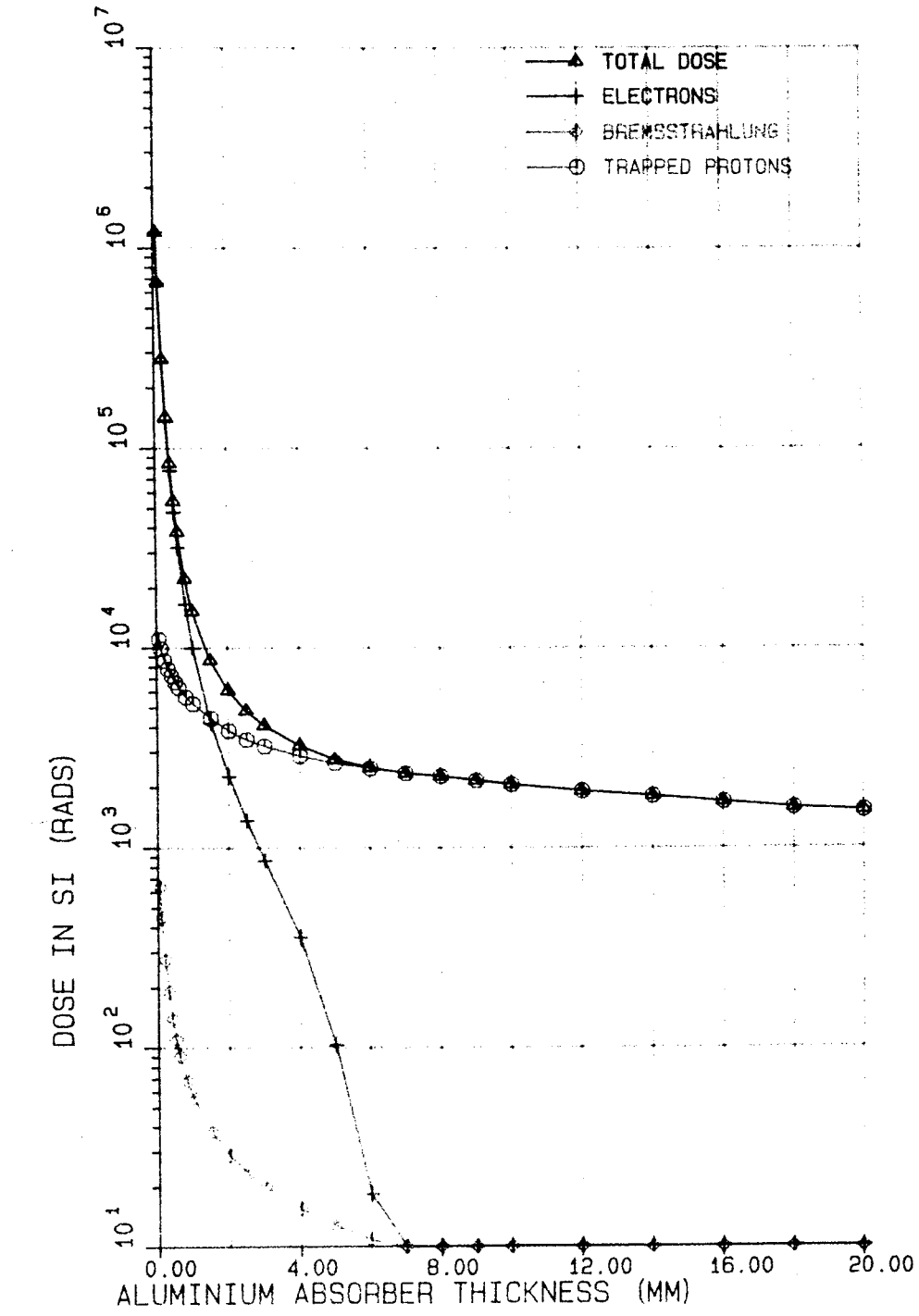

Annual dose as a function of spherical aluminium shield thickness for Low Earth Orbit: 1000 km circular at 28.5 degrees inclination. Protons dominate the dose for shields greater than 2 mm thick. Computed with the SHIELDOSE program. Solar minimum environment models AE8MIN and AP8MIC were used.

FIGURE 16.19

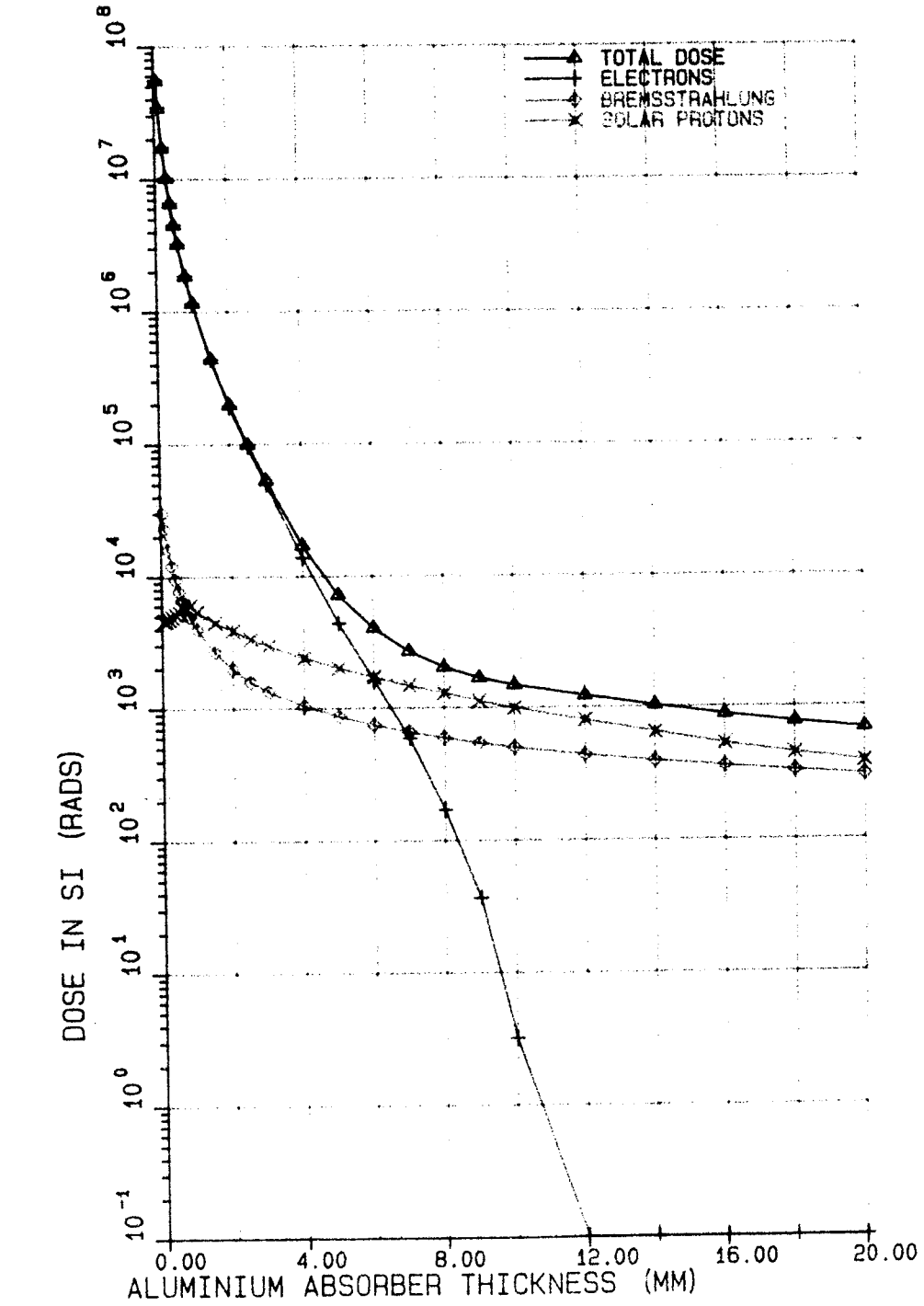

Annual dose as a function of spherical aluminium shield thickness for geostationary orbit: 35786 km circular equatorial. Electrons dominate the dose for shields less than 6 mm thick. Computed with the SHIELDOSE program. Solar maximum environment model AE8MAX and AP8MAC were used.

FIGURE 16.20

16.9.2. Radial-altitude profiles for dose and damage

The variation of orbit-integrated particle fluxes with altitude was discussed in Section 3, where "radial profiles" of electron and proton fluxes were shown. It is instructive to treat the resulting dose within shielding in a similar way. Figure 16.21 shows the radial profiles of dose accumulated in silicon within spherical aluminium of various thicknesses, (a) trapped electrons, (b) electron-induced bremsstrahlung, (c) trapped protons and (d) the total. These are for single circular equatorial orbits and are only included for illustrative purposes. The radiation-belt structure of the environment and the shielding effects on the various radiation species are clear.

Figures 16.22 and 16.23 give similar radial profiles of damage-equivalent 1 MeV electron flux in aluminium behind various thicknesses of aluminium for trapped electrons and protons. The belt structure is again shown. The concept of equivalent 1 MeV electron flux relates to atomic displacement damage and has been explained earlier. This particular effect is unlikely to be significant in the type of device which is the main concern of this document.

Dose and damage profiles calculated for orbits of high inclination show higher integrated doses at low altitude and a less pronounced minimum in the "slot" region (8000 km altitude). We can explain this with the example of a polar (90°) orbit. This cuts the horns of the outer belt (see Figure 3.2) four times per orbit. Orbits as low as 300 km pick up significant doses from these horns, whereas doses from the heart region are negligible at this altitude.

In Figure 16.24, some of the other useful features of radial dose profiles are also demonstrated. The dose profiles for 4 mm of aluminium absorber have been replotted; proton and electron doses have been summed. An attempt has also been made to give a visual guide to "no go" areas of space for specific spacecraft configurations.

The first point of interest demonstrated is that doses in low near-equatorial orbits are proton dominated. This dominance persists past the inner electron peak dose region at 3000 km and on to about 9000 km, after which the influence of protons is negligible. The outer peak region is electron-dominated and, surprisingly, yields the highest dose levels of all. Thus, for electronics, the least healthy "slot" in space appears to be around an altitude of 20000 km. For missions lasting more than one year, doses of over Megarad are possible.

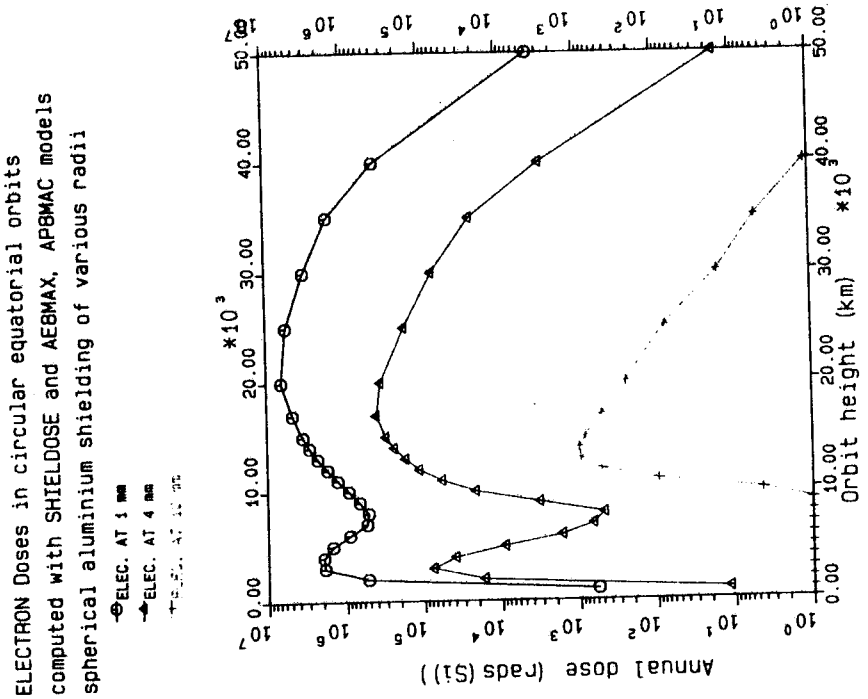

A

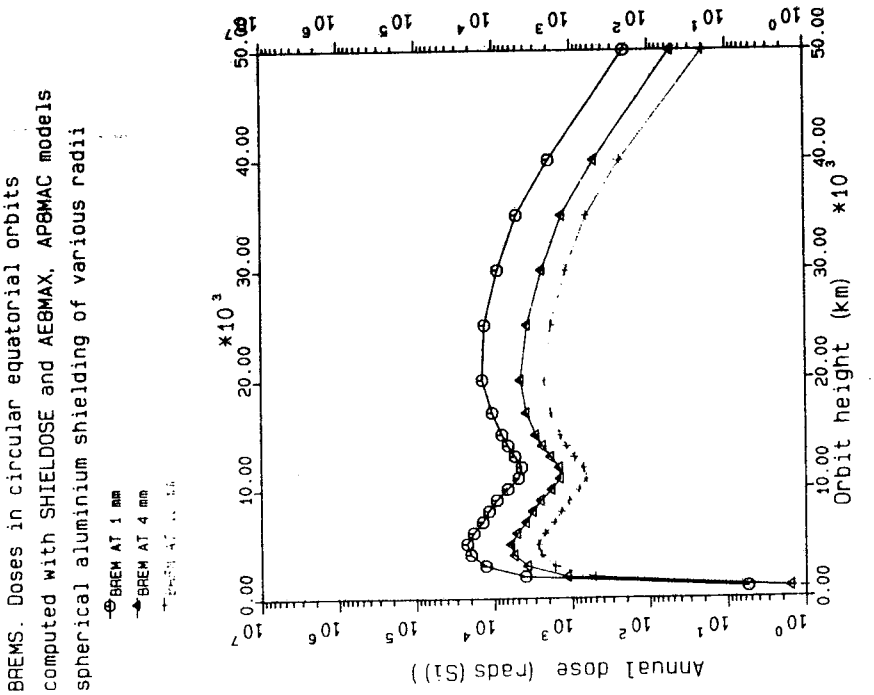

B

Radial doses (Si) profiles showing annual dose accumulated in silicon within spherical aluminium shields of thicknesses 1, 4 and 10 mm as functions of altitude of single circular equatorial orbits. (a) due to trapped electrons, (b) due to electron-induced bremsstrahlung,..

FIGURE 16.21

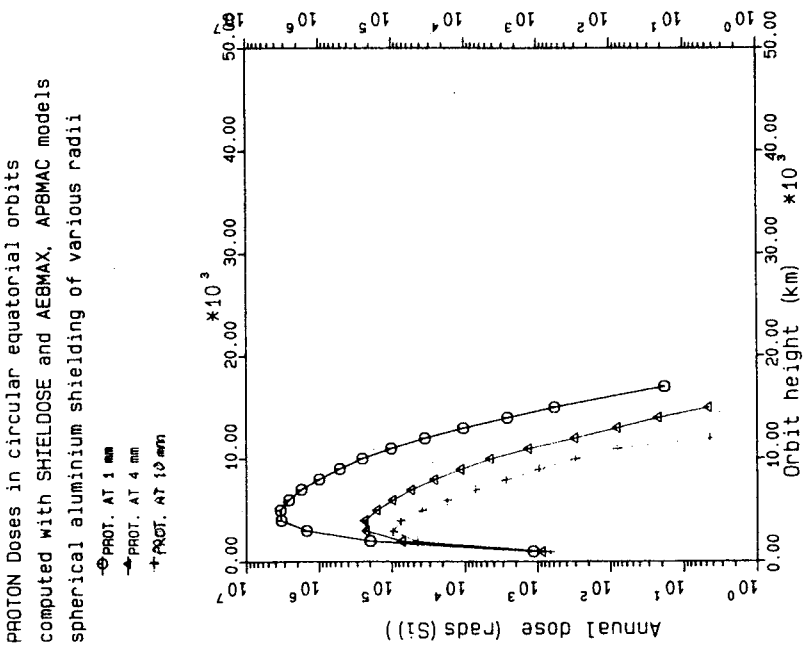

C

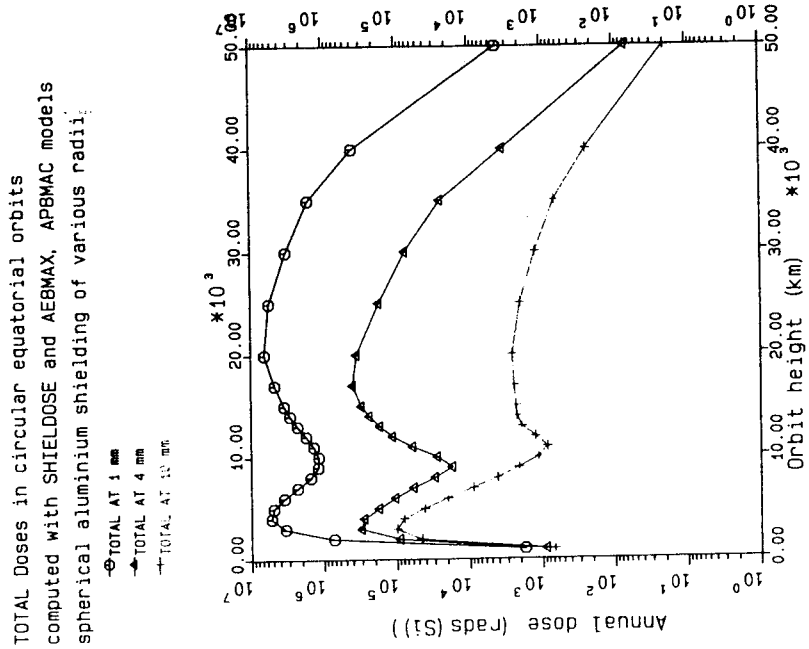

D

(c) due to trapped protons (d) total dose

FIGURE 16.21 (continued)

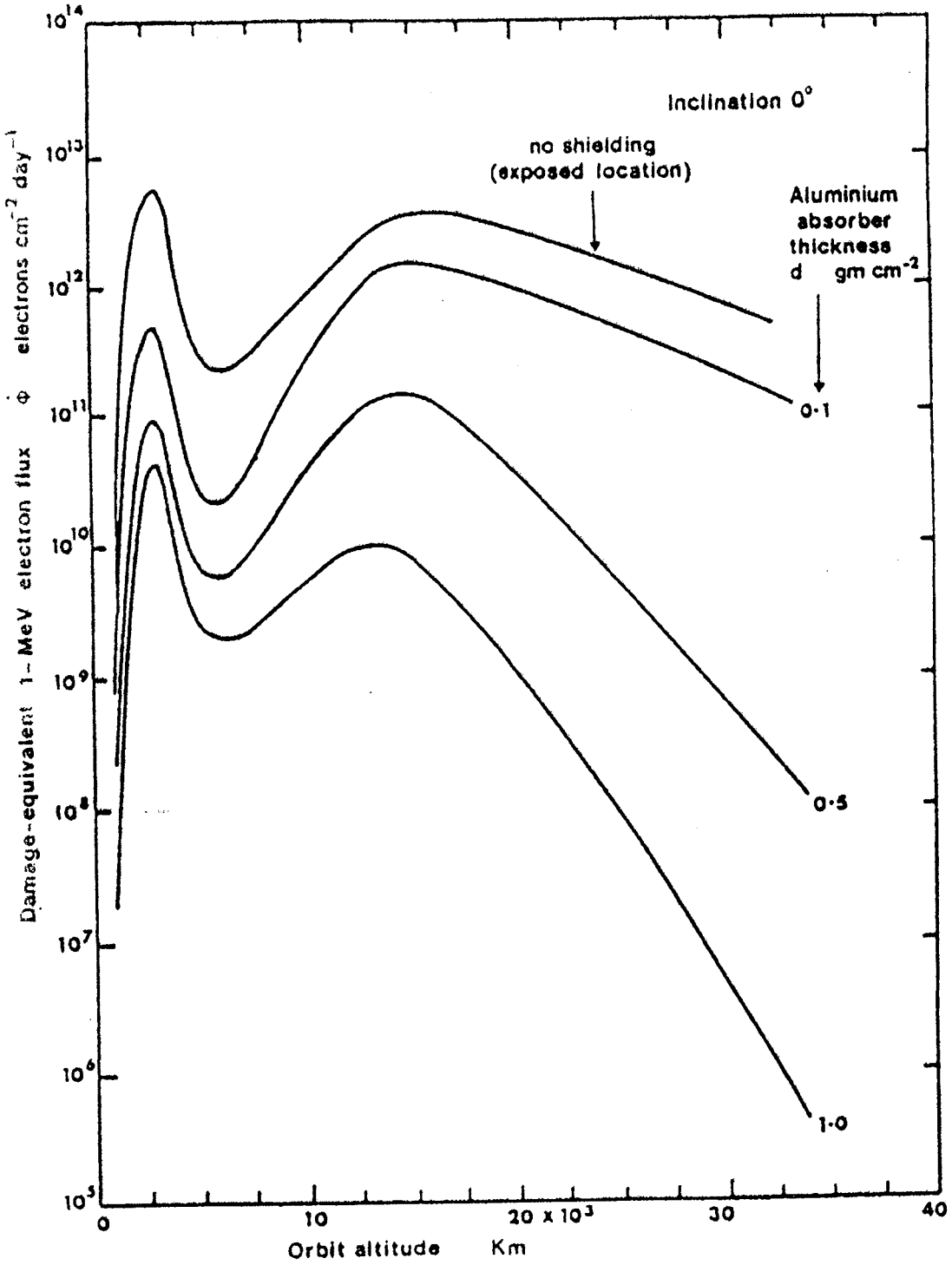

The damage-equivalent 1 MeV electron flux resulting from the trapped electron environment behind various thickness of aluminium absorber as a function of altitude in a circular equatorial orbit. AE-2 environment model.

FIGURE 16.22 - ELECTRON DAMAGE RADIAL-ALTITUDE PROFILES

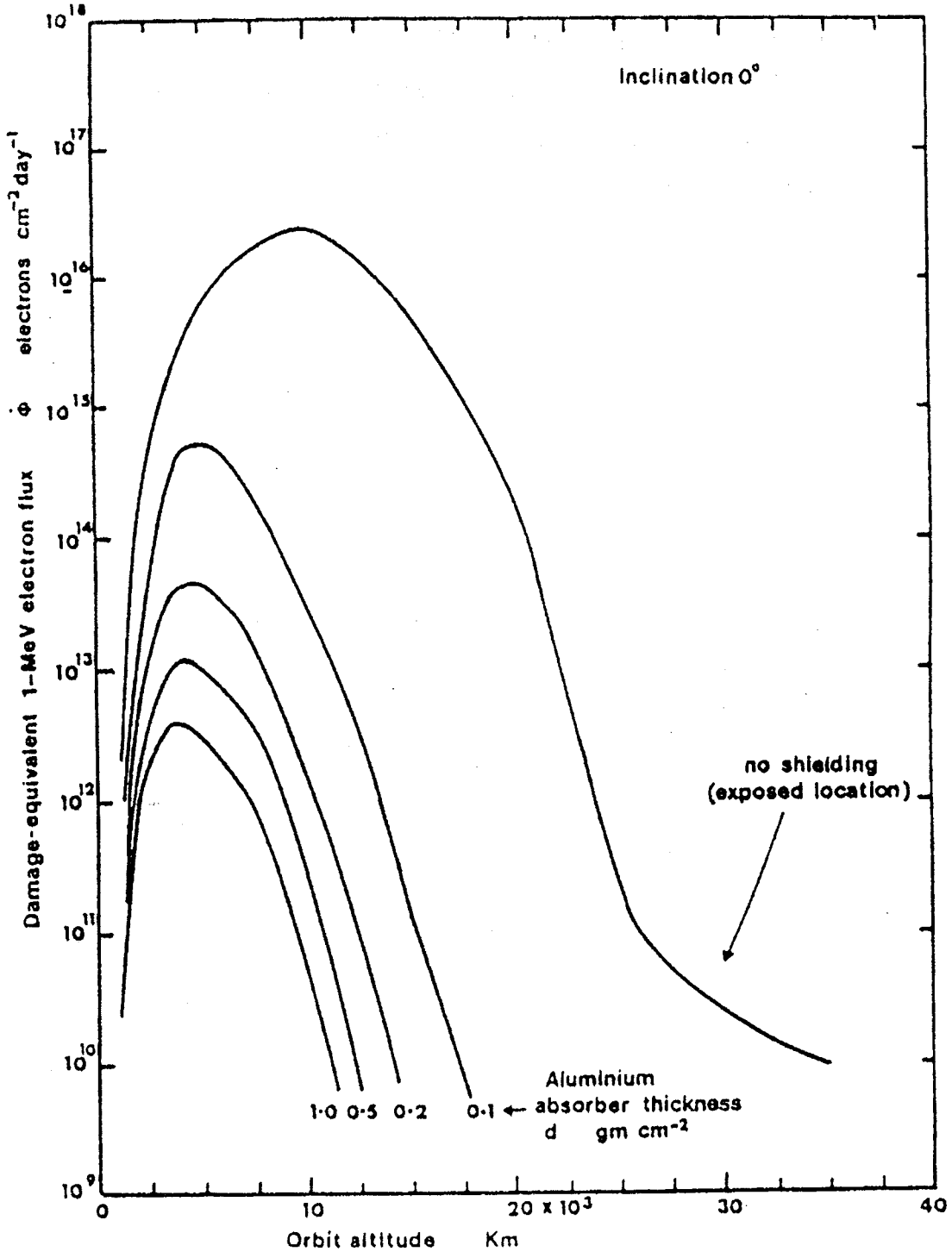

The damage-equivalent 1 MeV electron flux resulting from the trapped proton environment behind various thickness of aluminium absorber as a function of altitude in a circular equatorial orbit. AE-2 environment model.

FIGURE 16.23 - PROTON DAMAGE RADIAL-ALTITUDE PROFILES

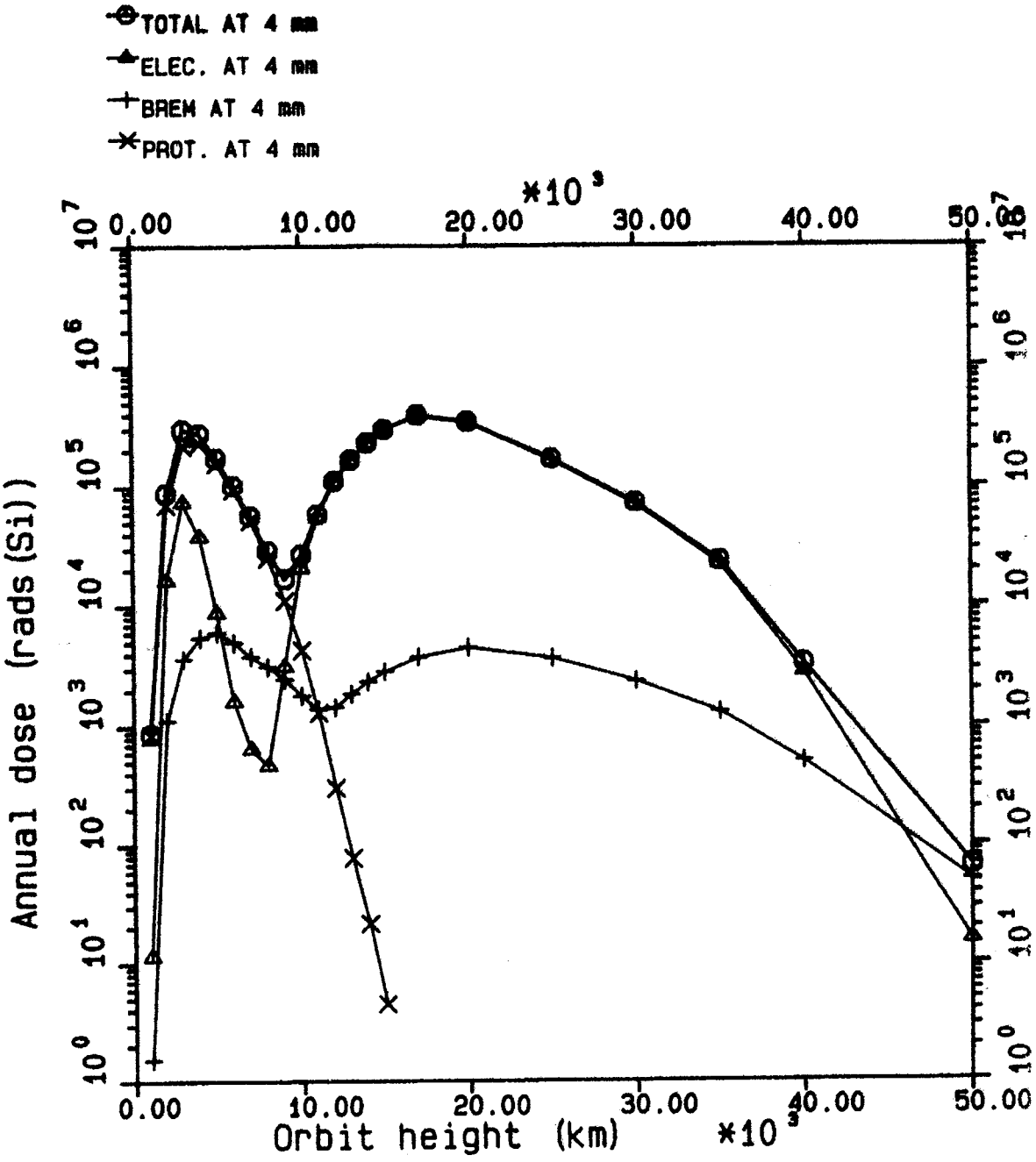

Annual doses (Si) within 4 mm special aluminium shielding as functions of altitude. Contributions from electrons, bremsstrahlung and protons are shown.

FIGURE 16.24

16.10 Nuclear reactions and other effects

Most of the mechanisms involved in the transport of radiation in a medium dealt with thus far have concerned interactions mainly at the atomic or molecular level: ionisation is a removal of atomic electrons; bremsstrahlung is produced by electron scattering in atomic fields; displacement damage results from atoms from a solid lattice. A small fraction of the incident particle flux may penetrate to atomic nucleii of the medium and initiate a nuclear reaction. Although these interactions are infrequent compared to ionisation interactions, the results can be important. The nucleus may break apart with the fragments causing intense local ionisation, or it may emit secondary protons and neutrons, or it may stay for some time in an "excited" state, followed by a delayed emission or radiation (the material is then said to be "activated").

16.10.1. Proton-induced SEU/Latchup

When the result of a nuclear interaction is the break-up of the nucleus, the charged fragments usually have short range and, if the interaction occurs in a sensitive region of a logic device, may lead to single-event upset (SEU) or latchup like that caused by a heavy-ion's ionisation track. In-flight observations of the locations of spacecraft when on-board components exhibit SEU have shown that a significant fraction of the total number of events occurs while satellites are in the proton radiation belt. Upset rates on CRRES (Campbell, 1991) and UoSAT-2 (Harboe-Sorensen et al., 1990) were much higher in the proton belts than in regions of space exposed to cosmic rays alone. Moreover, the CRRES data appear to show that multiple upsets, where the charge generation "contaminates" more than one logic cell, are more likely in the proton environment.

McNulty et al. (1980) and Peterson (1981) provided some of the early analysis of the processes. Evaluation of the problem can be made using Monte-Carlo computer simulation methods where the products of the interaction are determined statistically on the basis of fragmentation cross-section data such as those from Silberberg et al. (1985). Knowing the energies and ion species of the products, one can compute the energy deposition in a region and the upset rate (e.g. Bion and Bourrieau, 1989).

As with ion-induced SEU, testing in a representative ground-simulation environment is vital to the evaluation process. Bendel and Petersen (1983) have described a method for making predictions of in-orbit proton-induced error-rate which is simple provided the upset cross-section of a device as a function of proton energy is available from ground-tests. Harboe-Sorensen et al. (1990) show that this is less easy in practice and can result in predictions in disagreement with in-flight observation.

Recently an instrument on the ERS-1 satellite failed as a result of latchup in a memory while the satellite was passing through the South Atlantic anomaly where the proton radiation belt comes to its lowest altitude (Adams et al., 1992). This, together with the CRRES, UoSAT and much other experience, indicates that proton-nuclear reaction effects are a very important part of the overall radiation hazard.

16.10.2. Radiation-induced detector backgrounds

Primary energetic particles and their secondaries also interfere with payloads, most notably with detectors on astronomy missions where they produce a 'background' signal which may not be distinguishable from the proton signal being counted or which can overload the detector system. All astronomy missions, from infrared (e.g. ISO), through visible (e.g. HST, Hipparcos [Clausen and Perryman], 1989, UV (e.g. IUE) and X-ray (e.g. Exosat, RoSAT, XMM [Danner, 1992] and AXAF) to γ–ray (e.g. GRO, Cos-B, Integral [Dyer et al., 1988]) wavelengths, are or will be affected. The interference mechanism can be one of several, including bremsstrahlung radiation generated by electron slowing in material, Cerenkov radiation emitted when relativistic particles passed through optical materials; and delayed emissions of gamma-rays from the nuclei of activated spacecraft materials.

16.11 CONCLUSIONS

This section has described some of the physical principles involved when radiation interacts with materials and has indicated the approaches required to estimate the dose deposited in a sensitive device material which is protected from the direct action of the radiation environment by other absorber or "shield" materials.

We have demonstrated the complexity of the physical processes and noted the approximations which may be necessary. We should note particularly that some approximations which may be justifiable in preliminary calculations, when order of magnitude is the main question, should be removed in later, detailed calculations where compromises between weight and life are required.

Later sections deal more specifically with practical aspects of spacecraft equipment and the computer methods recommended when a large number of calculations must be performed (e.g. for a compromise estimation) or when the engineering decisions in question demand accuracy outside the scope of the manual methods described.

REFERENCES

L. Adams, E.J. Daly, R. Harboe-Sorensen, R. Nickson, J. Haines, W. Schafer, M. Conrad, H. Griech, J. Merkel, T. Schwall and R. Henneck, "A Verified Proton Induced Latchup in Space", IEEE Trans. Nucl. Sci. NS-38, 6 (1992)

W.H. Barkas and M.J. Berger, "Tables of Energy Losses and Ranges of Heavy Charged Particles", NASA Publication 1113, pp. 103-107, National Academy of Sciences, National Research Council, Washington DC (1964)

M.J. Berger and S.M. Seltzer, "Tables of Energy Losses and Ranges of Electrons and Positrons", NASA Publication 1113, pp. 205-269, National Academy of Sciences, National Research Council, Washington DC (1964)

M.J. Berger and S.M. Seltzer, "Stopping Powers and Ranges of Electronics and Protons", NBSIR-82-2550A, National Bureau of Standards (1982)

M.J. Berger and S.M. Seltzer, "Additional Stopping Power and Range Tables for Protons, Mesons and Electrons", NASA SP-3036, Office of Technology Utilisation, Washington DC (1966)

M.J. Berger and S.M. Seltzer, "Penetration of Electrons and Associated Bremsstrahlung through Aluminium Targets", NASA SP-169, pp. 285-322, Office of Technology Utilisation, Washington DC (1968)

H.A. Bethe, Handb. Phys. 24(1), p. 273 (1933)

T. Bion and J. Bourrieau, "A Model for Proton-Induced SEU", IEEE Trans. Nucl. Sci. NS-36, 6 2281 (1989)

W.L. Brown, J.D. Gabbe and W. Rosenzweig, "Results of the Telstart Radiation Experiments", The Bell System Technical Journal 42(4), pp. 1505-1559 (1963)

G.J. Brucker, "Correlation of Radiation Damage in Silicon Transistors Bombarded by Electrons, Protons and Neutrons", Paper presented at Conf. on Radiation Effects in Semiconductors, Toulouse (March 1967)

H. Bucker and R. Facius, "Radiation Problems in Manned Spaceflight with a View Towards the Space Station", Acta Austronautica (1988)

A.B. Campbell, "SEU Flight Data from the CRRES MEP", IEEE Trans. Nucl. Sci., NS-38, 6, 1647 (1991)

J.B. Cladis, G.T. Davidson, and L.L. Newkirk (Eds), "The Trapped Radiation Handbook", Report DNA 2524H, General Electric Co., Santa Barbara (1973)

K.F. Clausen and M.A.C. Perryman, "The Hipparcos Mission", IAF Paper 89-459, 40th. International Astronautical Congress, Malaga, Oct. 1989

R.A. Cliff, V. Danchenko, E.G. Stassinopoulos, M. Sing, G.J. Brucker and R.S. Ohanian, "Prediction and Measurements of Radiation Damage to CMOS Devices on board Spacecraft", X-700-76-227, NASA Goddard SFC (Oct. 1976) and IEEE Trans.Nucl.Sci. NS-23(6), pp. 1781-1788 (Dec. 1976)

W.C. Cooley, and R.J. Janda, "Handbook of Space Radiation Effects on Solar Cell Power Systems", NASA SP-3003, U.S. Dept. of Commerce, Washington DC (1963)

R. Danner, "Charged Particle Induced Background Expected on XMM", Estec Working Paper EWP 1674, ESTEC/WMA, 1992

C.S. Dyer, P.R. Truscott, A.J. Sims, C. Cumber and N.D.A. Hammond, "Particle Transport Simulation for Spaceborne, NaI Gamma-ray Spectrometers", IEEE Trans. Nucl. Sci. NS-35, 6, 1407, 1988

T.B.M. Dyer, proton nuclear reading: Petersen E.L. "Nuclear Reactions in Semiconductors", IEEE Trans. Nucl. Sci NS-27, 6, 1494 (1980) N.L. Bendel and E.L. Petersen, "Proton Upsets in Orbit" IEEE Trans. Nucl. Sci NS-30, 6, 4481 (1983) Harboe Sorensen et al.

R. Harboe-Sorensen, E.J. Daly, C.I. Underwood, J. Ward and L. Adams, "The Behaviour of Measured SEU at Low Altitude During Periods of High Solar Activity", IEEE Trans. Nucl. Sci. NS-37, 6, 1990

A.C. Hardy, M.D. Lopez and T.T. White, Trans.Am.Nuclear Soc., 10, p. 383 (1967)

A.G. Holmes-Siedle and W. Poch, JBIS 24(5), p. 273 (1971)

A.G. Holmes-Siedle, ESA Contract AHS-EXO-77-1 (Febr. 1977)

A.G. Holmes-Siedle and R.F.A. Freeman, "Radiation Effects Handbook", ESA Contract Report No. CR(P)-1067, Fulmer Research Inst., Slough, U.K. (April 1978)

H.E. Johns and J.R. Cunningham, "The Physics of Radiology", Thomas (1971)

F.L. Keller and R.G. Pruett, "The Effect of Charged Particle Environments on Manned Military Space Systems", NASA SP-71, U.S. Dept. of Commerce, Washington DC (1965)

D.W. Kingsland, Private communication

G.F. Knoll, "Radiation Detection and Measurement", Second edition, John Wiley and Sons, New York, 1989

V.J.L. Linnenbom, NRL Report 5828 (1962)

B.W. Mar, Nuclear Science and Engineering 24, pp. 193-199 (1966)

P.J. McNulty, G.E. Farrell, R.C. Wyatt, P.L. Rothwell, R.C. Filtz and J.N. Bradford, "Upset Phenomena Induced by Energetic Protons and Electrons", IEEE Trans. Nucl. SCI NS27(6) (1980)

E.L. Petersen and W.L. Bendel, " Protons Upsets in Orbit", IEEE Trans. Nucl. SCI NS30(6) (1983)

E. Peterson, "Soft Errors due to Protons in the Radiation Belt", IEEE Transactions on Nuclear Science, NS28(6), (Dec. 1981)

W. Poch, Private communication

S.M. Seltzer, Private communication, via M.J. Teague, NSSDC

S.M. Seltzer, "Electron, Electron-Bremsstrahlung and Proton Depth-Dose Data for Space Shielding Applications", IEEE Trans. Nucl. SCI NS26(6) (1979)

R. Silberberg, C.H. Tsao and J.R. Letaw, "Improved Cross Section Calculations for Astrophysical Applications", Astrophys. J. Suppl. 58, 873 (1985)

J.R. Srour, S. Othmer and K.V. Chiu, ibid., pp. 2656-2662

H.Y. Tada, J.R. Carter, B.E. Ansprangh and R.G. Downing, "Solar Cell Radiation Handbook", JPL Publication 82-69 (1982)

M.J. Teague, Private communication

V.A.J. Van Lint, G. Gigas and J. Barengoltz, IEEE Trans.Nucl.Sci. NS-22(6), pp. 2663-2668 (Dec. 1975)

K.A. Wright and J.G. Trump, J.Appl.Phys. 33, p. 687 (1962)

S.J. Wyard, Proc.Phys.Soc. A65, p. 377 (1952)

W.R. Yucker and J.R. Lilley, "Charge Code for Space Radiation Shielding Analysis", Report DAC-62231, McDonnell Douglas Astronautics Co. (1969)